

Topological Invariant and Edge States of Generalized Fully Nonlinear Schrödinger Equations

Di Zhou*

School of Physics, Beijing Institute of Technology, Beijing, 100081, China
School of Physics, Georgia Institute of Technology, Atlanta, GA 30332, USA and
Department of Physics, University of Michigan, Ann Arbor, MI 48109-1040, USA

Despite the extensive studies of topological states, its characterization in fully nonlinear classical systems has been lacking. In this work, we identify the proper definition of Berry phase of nonlinear bulk modes and characterize topological phases in one-dimensional (1D) generalized nonlinear Schrödinger equations in fully nonlinear regime, where the nonlinear parts of interactions are comparable to the linear ones. Without utilizing linear analysis, we develop an analytic strategy to demonstrate the quantization of Berry phase due to reflection symmetry. Interestingly, the lattice encounters a topological phase transition controlled by nonlinear bulk mode amplitudes. We then show nonlinear extension of bulk-edge correspondence by identifying topological boundary modes. We propose two classical structures that can be experimentally implemented. Our work opens the door to the rich physics between topological phases of matter and nonlinear dynamics.

I. INTRODUCTION

The advent of topological band theory[1–5] has led to the burgeoning field of “topological phases of matter” which manifest exotic properties, such as surface conduction of electronic states, and wave propagation insensitive to backscattering and disorder. In classical structures[6–13], enormous efforts have been devoted to emulate topological states and enable many pioneering applications[14–18].

To date, most of the studies of classical structures have been limited to linear topological band theory, with a few exceptions in weakly nonlinear regime[8, 19–21] where perturbation theory is available. In 1D problems, the wave functions are sinusoidal in time, and the topological invariant called Berry phase[22] is quantized by symmetries expressed as matrix operators. Due to bulk-edge correspondence, topologically protected evanescent modes emerge on lattice boundaries. Despite the rich topological physics in linear systems, nonlinear dynamics are more ubiquitous in nature, such as biochemical processes[23], fluid dynamics[24], and metamaterials[25, 26], etc. They give rise to unconventional properties like bifurcation[27], instability, solitons[28], and chaos[29, 30]. The question naturally arises: whether topological invariants and phases can be extended to nonlinear systems?

In this paper, we present a systematic study of topological attributes in 1D generalized nonlinear Schrödinger equations[8, 31, 32]. The nonlinear parts of interactions are comparable to the linear ones and perturbation theory breaks down, which we designate the “fully nonlinear regime”. We limit our considerations within the amplitude range[33, 34] that chaos does not occur. Consequently, nonlinear bulk modes[35, 36] are remarkably distinct from sinusoidal waves (e.g., figs.1(b) and 3(d)). We develop the proper definition of Berry phase

in nonlinear bulk modes. By adopting a symmetry-based analytic treatment, we demonstrate the quantization of Berry phase in reflection-symmetric systems, regardless of the availability of linear analysis. The emergence of nonlinear topological boundary modes is associated with quantized Berry phase and they are insensitive to disorders. Finally, we identify zero-frequency topological modes in nonlinear systems analogous to models subjected to charge-conjugation symmetry.

II. QUANTIZED BERRY PHASE OF NONLINEAR BULK MODES

Generalized nonlinear Schrödinger equations are widely studied in classical systems like nonlinear optics[15, 31], electric circuits[8], and mechanical structures[34]. Their equations of motion are summarized as the general form in Eqs.(1) below. We study nonlinear bulk modes, from which we define Berry phase and demonstrate its quantization in reflection-symmetric models.

The considered model is a nonlinear SSH[28] chain composed of N classical dimer fields $\Psi_n = (\Psi_n^{(1)}, \Psi_n^{(2)})^\top$ (\top is matrix transpose) coupled by nonlinear interactions. The chain dynamics is governed by the 1D generalized nonlinear Schrödinger equations,

$$\begin{aligned} i\partial_t \Psi_n^{(1)} &= \epsilon_0 \Psi_n^{(1)} + f_1(\Psi_n^{(1)}, \Psi_n^{(2)}) + f_2(\Psi_n^{(1)}, \Psi_{n-1}^{(2)}), \\ i\partial_t \Psi_n^{(2)} &= \epsilon_0 \Psi_n^{(2)} + f_1(\Psi_n^{(2)}, \Psi_n^{(1)}) + f_2(\Psi_n^{(2)}, \Psi_{n+1}^{(1)}), \end{aligned} \quad (1)$$

subjected to periodic boundary condition (PBC), where $\epsilon_0 \geq 0$ is the on-site potential, $f_i(x, y)$ are real-coefficient general polynomials of x, x^*, y , and y^* ($*$ represents complex conjugate), and $f_i(x, y)$ for $i = 1$ and $i = 2$ stand for intracell and intercell nonlinear couplings, respectively.

In linear regime, the polynomials are approximated as $f_i(x, y) \approx c_i y$ ($c_{i=1,2} > 0$) to have “gapped” two-band models when $c_1 \neq c_2$. The bulk modes are sinusoidal

* Corresponding author: dizhou@bit.edu.cn

in time, and Berry phase is quantized by reflection symmetry. The nonlinearities become increasingly important as the bulk mode amplitude rises. In the “fully nonlinear regime” where nonlinear interactions become comparable to the linear ones, nonlinear bulk modes are remarkably different from sinusoidal waves (e.g. figs.1(b), 3(b), and 3(d)), and the eigenfrequencies naturally deviate from their linear counterparts. Hence, we define nonlinear band structure[8, 19] $\omega = \omega(q \in [0, 2\pi], A)$ as the eigenfrequencies of nonlinear bulk modes for given amplitude A . We consider the simple case that nonlinear bulk modes are always non-degenerate (i.e., different ω for different modes) unless they reach the topological transition amplitude when the nonlinear bands merge at the band-touching frequency. Hence, given the amplitude, frequency, and wavenumber, a nonlinear bulk mode is uniquely defined. Extended from gapped linear models, the lattice is a “gapped two-band nonlinear model”. In what follows, we define Berry phase for nonlinear bulk modes of the upper-band by adiabatically evolving wavenumber which traverses the Brillouin zone.

The considered nonlinear bulk mode, denoted as

$$\Psi_q = (\Psi_q^{(1)}(\omega t - qn), \Psi_q^{(2)}(\omega t - qn + \phi_q))^\top, \quad (2)$$

is periodic in time, where ω and q are the frequency and wavenumber, respectively. $\Psi_q^{(j)}(\theta)$ ($j = 1, 2$) are 2π -periodic wave components, where the phase conditions are chosen by asking $\text{Re} \Psi_q^{(j)}(\theta = 0) = A$, and $A \stackrel{\text{def}}{=} \max(\text{Re} \Psi_q^{(j)})$ is the amplitude. Consequently, ϕ_q characterizes the relative phase between the two wave components. Nonlinear bulk modes are not sinusoidal. They fulfill $i\partial_t \Psi_q = H(\Psi_q)$, where $H(\Psi_q)$ is the nonlinear differential operator obtained from Eqs.(1) and is elaborated in App.A. Given the amplitude A of nonlinear bulk mode, we find that ω , ϕ_q , and waveform are governed by wavenumber q .

We realize the adiabatic evolution of wavenumber $q(t')$ traversing the Brillouin zone from $q(0) = q$ to $q(t) = q + 2\pi$, while the amplitude A remains unchanged during this process. According to the nonlinear extension of adiabatic theorem[37–40], a system $H(\Psi_q)$ initially in one of its eigenmode Ψ_q will stay as an instantaneous eigenmode of $H(\Psi_{q(t)})$ throughout this procedure, provided that the nonlinear eigenmode Ψ_q is stable[39] within the amplitude scope of this paper. The stability of nonlinear bulk modes is confirmed in App.C via the algorithm of self-oscillation[12, 21, 36]. Therefore, the only degree of freedom is the phase of eigenmode. At time t , the eigenmode is $\Psi_{q(t)}(\int_0^t \omega(t', q(t')) dt' - \gamma(t))$. After traversing the Brillouin zone, the wave function acquires an extra phase γ expressed as follows,

$$\gamma = \oint_{\text{BZ}} dq \frac{\sum_{l \in \mathcal{Z}} \left(l |\psi_{l,q}^{(2)}|^2 \frac{\partial \phi_q}{\partial q} + i \sum_j \psi_{l,q}^{(j)*} \frac{\partial \psi_{l,q}^{(j)}}{\partial q} \right)}{\sum_{l' \in \mathcal{Z}} l' \left(\sum_{j'} |\psi_{l',q}^{(j')}|^2 \right)}, \quad (3)$$

where the mathematical derivations are in App.A, $j, j' = 1, 2$ denote the two wave components, and $\psi_{l,q}^{(j)} =$

$(2\pi)^{-1} \int_0^{2\pi} e^{il\theta} \Psi_q^{(j)}(\theta) d\theta$ is the l -th Fourier component of $\Psi_q^{(j)}$. γ is dubbed Berry phase of nonlinear bulk modes. In general, γ is *not quantized* unless additional symmetry properties are imposed on the model, which we will discuss below. We note that the eigenmodes of linear problems are sinusoidal in time, which reduces Eq.(3) to the conventional form[37] $\gamma = \oint_{\text{BZ}} dq i \langle \Psi_q | \partial_q | \Psi_q \rangle$.

Now we demonstrate that Berry phase defined in Eq.(3) is quantized by reflection symmetry. The model in Eqs.(1) respects reflection symmetry, which means that the nonlinear equations of motion are invariant under reflection transformation,

$$(\Psi_n^{(1)}, \Psi_n^{(2)}) \rightarrow (\Psi_{-n}^{(2)}, \Psi_{-n}^{(1)}). \quad (4)$$

Given a nonlinear bulk mode Ψ_q in Eq.(2), reflection transformation demands a partner solution

$$\Psi'_{-q} = (\Psi_q^{(2)}(\omega t + qn), \Psi_q^{(1)}(\omega t + qn - \phi_q))^\top \quad (5)$$

that also satisfies the model. On the other hand, a nonlinear bulk mode of wavenumber $-q$ is by definition denoted as $\Psi_{-q} = (\Psi_{-q}^{(1)}(\omega t + qn), \Psi_{-q}^{(2)}(\omega t + qn + \phi_{-q}))^\top$. Since there is no degeneracy of nonlinear bulk modes, Ψ'_{-q} and Ψ_{-q} have to be identical, which imposes the constraints

$$\phi_{-q} = -\phi_q \pmod{2\pi}, \quad (6)$$

and

$$\Psi_q^{(2)} = \Psi_{-q}^{(1)} \xrightarrow{\text{Fourier transform}} \psi_{l,q}^{(2)} = \psi_{l,-q}^{(1)}. \quad (7)$$

Eqs.(6, 7) are the mathematical formalism of reflection symmetry, and they are the key to quantize Berry phase in Eq.(3),

$$\gamma = \frac{1}{2} \oint_{\text{BZ}} \frac{d\phi_q}{dq} dq = \phi_\pi - \phi_0 = 0 \text{ or } \pi \pmod{2\pi}, \quad (8)$$

where the details are elaborated in App.B. Here, ϕ_0 and ϕ_π are the relative phases of the upper-band nonlinear modes at high-symmetry points $q = 0$ and π , respectively. They are determined by comparing the eigenfrequencies $\omega(\phi_q = 0)$ and $\omega(\phi_q = \pi)$ at $q = 0$ and π . Specifically, $\gamma = \pi$ if $\omega(\phi_0 = 0)$ and $\omega(\phi_\pi = \pi)$ belong to the upper band, whereas $\gamma = 0$ if $\omega(\phi_0 = 0)$ and $\omega(\phi_\pi = 0)$ are in the upper band. Interestingly, the lattice encounters a topological transition induced by the critical amplitude $A = A_c$ when eigenfrequencies merge at $\omega(\phi_\pi = 0, A_c) = \omega(\phi_\pi = \pi, A_c)$. The nonlinear bandgap reopens above A_c with an abrupt change of Berry phase. This transition is exemplified by the minimal model of nonlinear topological lattice in Sec.III.

Having established quantized Berry phase, we now search additional properties for vanishing on-site potential, $\epsilon_0 = 0$. In linear counterpart, the model respects charge-conjugation symmetry[5, 6] which demands the eigenstates to appear in $\pm\omega$ pairs, and the topological mode to have zero-energy. To have $\pm\omega$ pairs of eigenmodes in the nonlinear problem, we ask the parity of interactions to yield $f_i(-x, y) = -f_i(x, -y) = f_i(x, y)$.

Consequently, the system is invariant under the transformation

$$(\Psi_n^{(1)}(\omega t), \Psi_n^{(2)}(\omega t)) \rightarrow (-\Psi_n^{(1)}(-\omega t), \Psi_n^{(2)}(-\omega t)). \quad (9)$$

Given a nonlinear mode Ψ_ω defined in Eq.(2) with the frequency ω , this transformation demands a partner solution of frequency $-\omega$,

$$\Psi_{-\omega} = (-\Psi_q^{(1)}(-\omega t - qn), \Psi_q^{(2)}(-\omega t - qn + \phi_q))^\top. \quad (10)$$

Therefore, nonlinear eigenmodes always appear in $\pm\omega$

pairs. Similar to charge-conjugation symmetric models in linear systems[5], the eigenfrequencies of nonlinear topological modes are zero, which is illustrated in the following minimal model.

III. TOPOLOGICAL TRANSITION AND BULK-EDGE CORRESPONDENCE IN THE MINIMAL MODEL

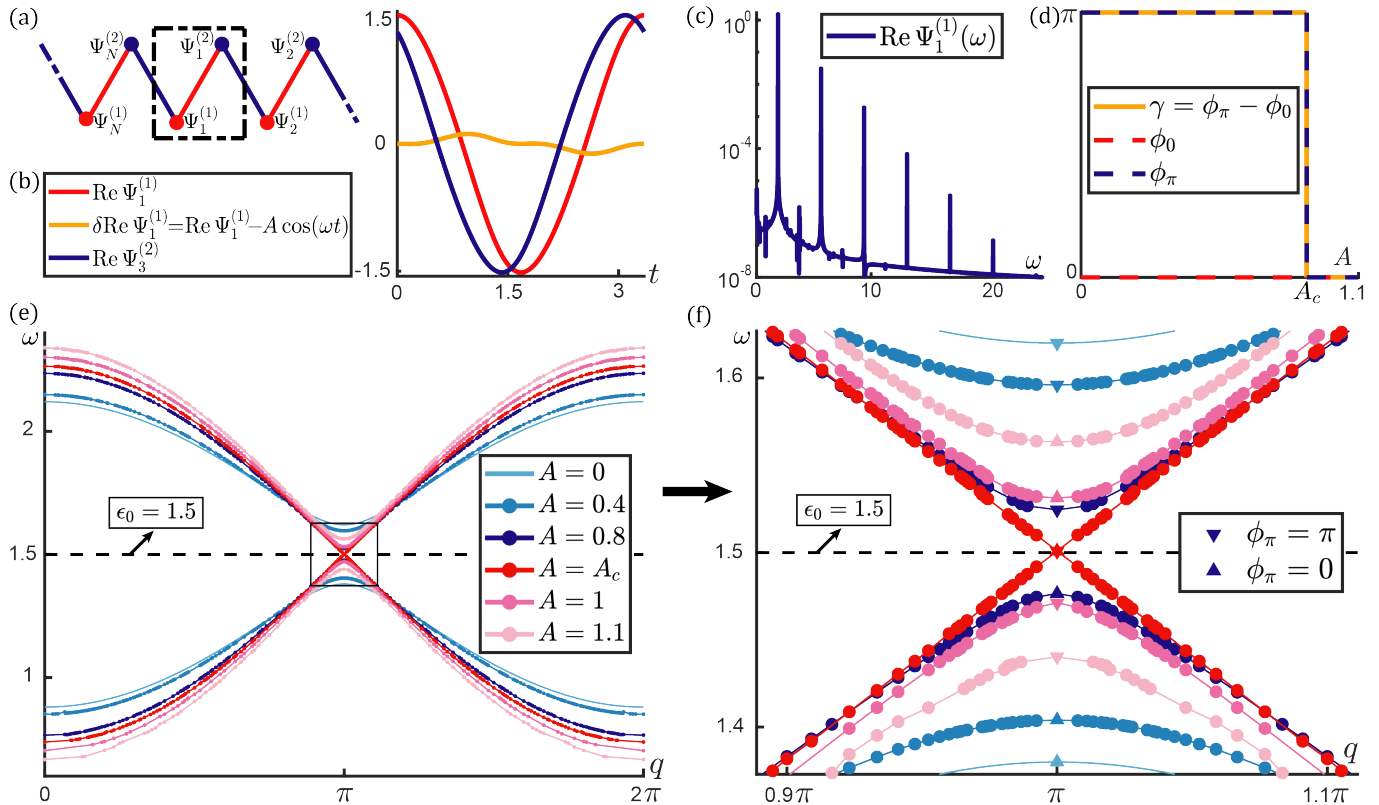


FIG. 1. The minimal model of nonlinear SSH chain. The parameters are $\epsilon_0 = 1.5$, $c_1 = 0.25$, $c_2 = 0.37$, $d_1 = 0.22$, and $d_2 = 0.02$. (a) Schematic illustration of the lattice subjected to PBC. Unit cell is enclosed by black dashed box. Red and blue bonds represent intracell and intercell couplings. (b) A nonlinear bulk mode computed by *shooting method*[41–43] with amplitude $A = 1.5$ and wavenumber $q = 4\pi/5$. Red and blue curves are the wave functions of $n = 1$ and 3 sites, respectively. The nature of bulk modes is exhibited by their equal amplitudes. Orange curve shows the noticeable difference between nonlinear mode and sinusoidal function. (c) Frequency profile of nonlinear bulk mode in (b). It additionally verifies the mode deviations from sinusoidal functions. (d) Berry phase of the upper nonlinear band as the function of amplitude. $\phi_0 = 0$ does not change because there is no band-touching at $q = 0$, whereas ϕ_π and γ experience a jump at band-touching point A_c for wavenumber $q = \pi$. (e) Nonlinear band structures $\omega = \omega(q, A)$ plotted for bulk mode amplitudes from $A = 0$ to 1.1 . The red curves touch for the topological transition amplitude $A_c = 0.8944$ at $\omega = \epsilon_0 = 1.5$. It is worth of emphasizing that $A_c^2 \max(d_1, d_2) / \max(c_1, c_2) \approx 0.5$, which demonstrates the comparable nonlinear and linear interactions in fully nonlinear regime. Black box encircles band structures around transition point which is elaborated in (f). (f) Enlarged nonlinear band structures near band-touching point for a list of amplitudes in (e). ∇ and \triangle mark antisymmetric and symmetric modes at $q = \pi$, respectively. Topological transition occurs when they merge at $A = A_c$.

We now clarify the nonlinear extension of bulk-edge

correspondence by demonstrating topological boundary

modes in the minimal model, where the couplings are specified as

$$f_i(x, y) = c_i y + d_i[(\text{Re } y)^3 + i(\text{Im } y)^3], \quad (11)$$

with $c_i, d_i > 0$ for $i = 1, 2$. We are interested in attributes unique in nonlinear systems, namely topological phase transition induced by bulk mode amplitudes. Thus, the parameters yield $c_1 < c_2$ and $d_1 > d_2$. We study two cases: $\epsilon_0 \neq 0$ and $\epsilon_0 = 0$. In the rest of the paper, a semi-infinite lattice subjected to open boundary condition (OBC) is always considered whenever we refer to topological boundary modes.

First, we consider the case described by Eqs.(1) with $\epsilon_0 \neq 0$, which intrinsically possesses reflection symmetry.

Given that Berry phase $\gamma(A = 0) = \pi$, the lattice is topologically nontrivial in the linear limit. As amplitudes rise, the topological invariant $\gamma(A < A_c) = \pi$ cannot change until it becomes ill-defined when the nonlinear bandgap closes at the transition amplitude A_c . The bandgap reopens above A_c , allowing the well-defined Berry phase to take the trivial phase $\gamma(A > A_c) = 0$ (see fig.2(d)). A_c is numerically computed by solving the bandgap-closing equation $\omega(\phi_\pi = 0, A_c) = \omega(\phi_\pi = \pi, A_c)$. We propose a convenient approximation[44] $f(\Psi_{n'}^{(j')}, \Psi_n^{(j)}) \approx (c_i + \frac{3}{4}d_i A^2)\Psi_n^{(j)}$ to estimate the transition amplitude $A_c \approx \sqrt{4/3}a_c$, where $a_c = \sqrt{-(c_2 - c_1)/(d_2 - d_1)}$. The good agreement between this approximation and the numerical solutions is shown in App.C.

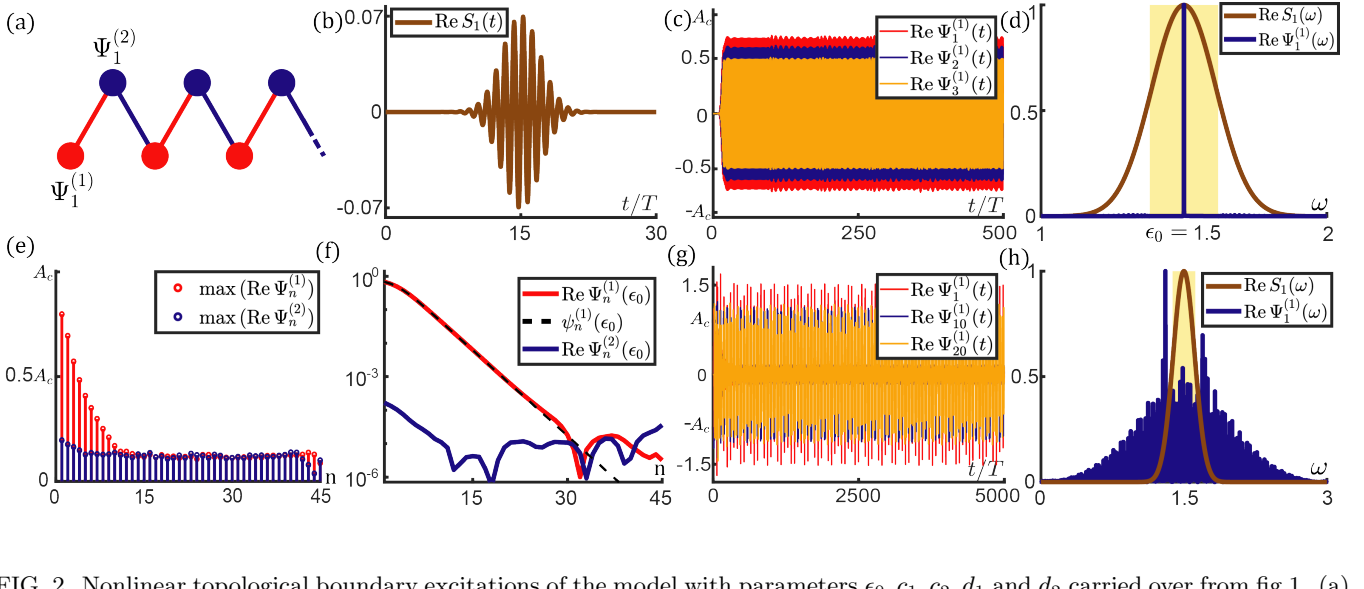


FIG. 2. Nonlinear topological boundary excitations of the model with parameters $\epsilon_0, c_1, c_2, d_1$ and d_2 carried over from fig.1. (a) A chain composed of $N = 45$ unit cells is subjected to OBCs on both ends to mimic a semi-infinite lattice. (b) A Gaussian tone burst $S_n(t) = \delta_{n1} S e^{-i\omega_{\text{ext}} t - (t-t_0)^2/\tau^2} (1, 0)^\top$ applied at $n = 1$ site to trigger nonlinear topological boundary modes. The signal amplitude $S = 7 \times 10^{-2}$, the carrier frequency $\omega_{\text{ext}} = \epsilon_0 = 1.5$, the period $T = 2\pi/\omega_{\text{ext}}$, $\tau = 3T$, and $t_0 = 15T$. (c) Responding wave functions of $n = 1, 2, 3$ sites. They indicate the localization of nonlinear topological modes, where the mode amplitude $\max(\text{Re } \Psi_1^{(1)}) < A_c$. (d) Brown curve is the frequency spectrum of Gaussian shaking normalized by shaking amplitude. Blue curve is the frequency spectrum of responding mode at site $n = 1$ normalized by its peak. Yellow shaded area stands for linear bandgap $|\epsilon_0 + c_1 - c_2| < \omega < |\epsilon_0 - c_1 + c_2|$. (e) Spatial profile of the amplitudes manifests bulk mode excitations. These bulk modes are excited by Gaussian signal containing all frequencies. (f) Red and blue curves represent the spatial profile of the $\omega = \epsilon_0$ wave component of the excitation, where $\Psi_n^{(1)}(\epsilon_0) \gg \Psi_n^{(2)}(\epsilon_0)$ is numerically verified here. The analytic prediction of the topological mode $\psi_n^{(1)}(\epsilon_0)$ is depicted by the black dashed curve, which is perfectly in alignment with numerical results. The flattened curve near lattice boundary indicates nonlinear effects. (g) The strength of external Gaussian shaking increased to $S = 56 \times 10^{-2}$ to excite a nonlinear mode of amplitude $A > A_c$. Wave functions for sites $n = 1, 10, 20$ are plotted. Their amplitudes are roughly equal, revealing bulk mode excitations. (h) Frequency spectrum of the mode in (g) normalized by the peak of the spectrum.

In linear problems, bulk-edge correspondence states that topologically protected boundary modes are guaranteed by the invariant derived from the bulk bands. In the nonlinear problem, we utilize analytic approximation and numerical experiment, to doubly confirm this the-

orem by identifying topological edge modes. The topological mode and eigenfrequency are denoted as $\Psi_n = (\Psi_n^{(1)}, \Psi_n^{(2)})^\top$ and ω_T , respectively. Analogous to linear SSH chain[28], the analytic scheme is to approximate

$\Psi_n^{(1)} \gg \Psi_n^{(2)}$, which is numerically verified in fig.2(f). We make one further approximation to truncate the equations of motion to fundamental harmonics. By doing so, we find $\omega_T = \epsilon_0$, and

$$c_1 \left(\frac{\sqrt{3}}{2} \psi_{1,n}^{(1)} \right) |\psi_{1,n}^{(1)}| = c_2 \left(\frac{\sqrt{3}}{2} \psi_{1,n+1}^{(1)} \right) |\psi_{1,n+1}^{(1)}|, \quad (12)$$

where $c_i(x) = c_i + d_i|x|^2$, and $\psi_{1,n}^{(1)}$ is the fundamental harmonic part of $\Psi_n^{(1)}$. Consequently, the nonlinear topological boundary mode is approximated as $\Psi_n \approx (\psi_{1,n}^{(1)}, 0)^\top e^{-i\epsilon_0 t}$. The semi-infinite lattice hosts a topo-

logical evanescent mode when $|\psi_{1,1}^{(1)}| < \sqrt{4/3}a_c \approx A_c$, whereas no such mode exists for $|\psi_{1,1}^{(1)}| > \sqrt{4/3}a_c \approx A_c$. The eigenfrequency and waveform are perfectly in line with the analytic method of multiple-scale[33, 34, 36] in weakly nonlinear regime (App.D). The numerical scenario is accomplished by applying a Gaussian profile signal $S_n = \delta_{n1} S e^{-i\omega_{\text{ext}} t - (t-t_0)^2/\tau^2} (1, 0)^\top$ on the $n = 1$ site of the lattice, where τ controls the Gaussian spread and t_0 denotes the trigger time. The numerical results in fig.2 verify the nonlinear extension of bulk-edge correspondence by identifying the arrival (disappearance) of boundary excitations below (above) the critical amplitude A_c .

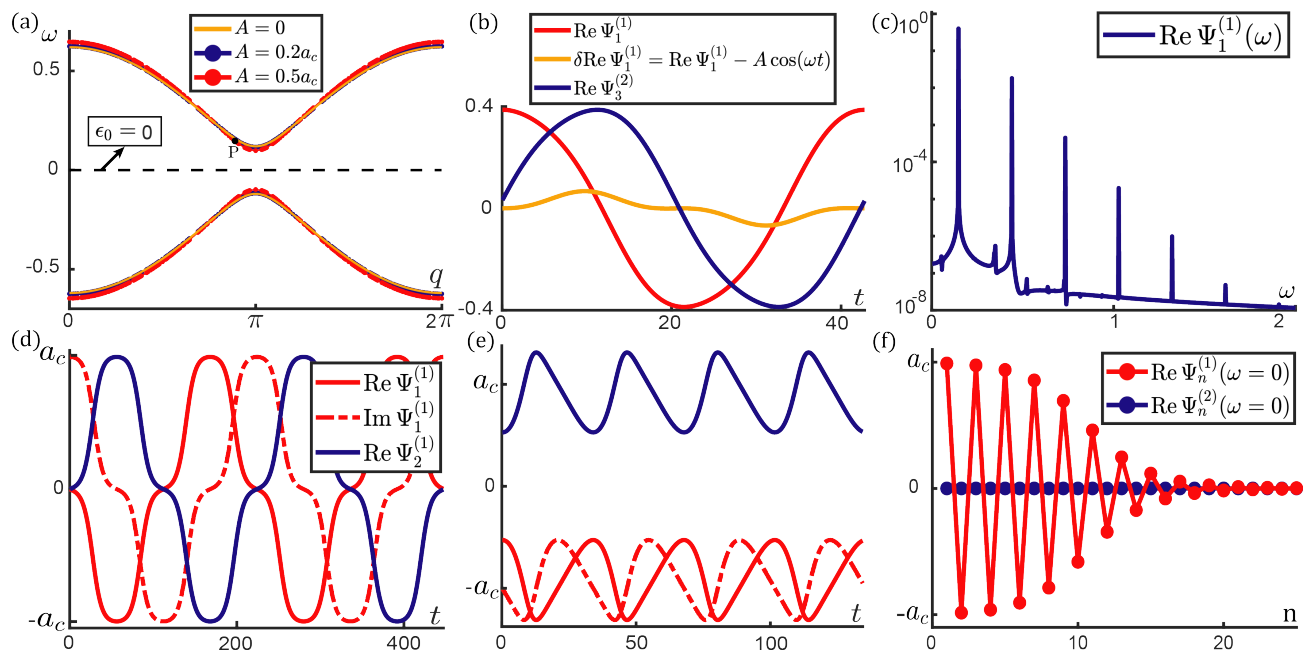


FIG. 3. The $\epsilon_0 = 0$ model with parameters c_1, c_2, d_1 and d_2 carried over from fig.1. (a) Nonlinear band structures exhibit bulk modes in $\pm\omega$ pairs from $A = 0$ to $0.5a_c$, where $a_c = 0.7746$. (b) Nonlinear bulk mode marked as P in (a) is obtained from shooting method, where $A = 0.5a_c$ and wavenumber $q = 8\pi/9$. Red and blue curves stand for the wave functions of $n = 1, 3$ sites. Orange curve indicates that the nonlinear mode is noticeably different from sinusoidal function. (c) Additional verification of such difference in (b) is offered by frequency spectrum of nonlinear bulk mode in (b). (d) A nonlinear bulk mode on the verge of instability, where the amplitude $A = 0.9877a_c \lesssim a_c$. (e) A nonlinear bulk mode with $\max |\text{Re } \Psi_n^{(1)}| = 1.312a_c > a_c$ experiences instability and oscillates around new ground states. (f) Spatial profile of static topological mode with amplitude $\text{Re } \Psi_1^{(1)} = 0.99a_c$. The associated stability analysis is in App.D.

One may find it unusual that the frequencies of topological modes $\omega_T = \epsilon_0$ are independent of the amplitudes, although this result is in agreement with Ref.[8, 19] in weakly nonlinear regime. Here we propose an explanation for this intriguing result. Because the evanescent mode fades to zero in the bulk, the “tail” of this mode eventually enters into small amplitude regime where nonlinearities are negligible and linear analysis becomes ef-

fective. Linear topological theory[28] demands the tail of the mode to be $\omega_T = \epsilon_0$, which in turn requests the frequency of the nonlinear topological mode to be independent of the amplitude.

Topological protection is featured in multiple aspects. As visualized in fig.1(e), the eigenfrequencies of topological modes stay in the bandgap and are distinct from nonlinear bulk modes. The appearance and absence of

these modes are captured by the topological invariant that cannot change continuously upon the variation of system parameters. Lastly, topological modes are insensitive to disorders, which is numerically verified in App.D.

In the second case with $\epsilon_0 = 0$, the model manifests nonlinear bulk modes in $\pm\omega$ pairs. Compared to the $\epsilon_0 \neq 0$ model, two additional properties emerge when $\epsilon_0 = 0$. The first property is that the lattice under PBC experiences instability when the amplitude $A = a_c$ and the nonlinear bands touch at zero frequency $\omega(\phi_\pi = 0, a_c) = \omega(\phi_\pi = \pi, a_c) = \epsilon_0 = 0$. The lattice reaches one of the eight new ground states described by the equilibrium wave functions $\Psi_n = (-1)^n \sqrt{2} a_c (e^{is_1 \pi/4}, s_2 e^{is_3 \pi/4})^\top$, where $s_1, s_2, s_3 = \pm 1$. The second peculiarity is that nonlinear topological modes appear static in time, from which we obtain exact solutions via the recursion relation, $f_1(\Psi_n^{(1)}, \Psi_n^{(2)}) + f_2(\Psi_n^{(1)}, \Psi_{n-1}^{(2)}) = f_1(\Psi_n^{(2)}, \Psi_n^{(1)}) + f_2(\Psi_n^{(2)}, \Psi_{n+1}^{(1)}) = 0$. In summary, this $\epsilon_0 = 0$ model is the nonlinear analog of charge-conjugation symmetric systems, in the sense that bulk modes appear in $\pm\omega$ pairs, and topological modes are static.

IV. PROPOSALS FOR EXPERIMENTAL IMPLEMENTATIONS

Upon establishing nonlinear topological band theory, it is natural to ask if any realistic physical systems enjoy these unconventional properties. Three classical structures are proposed here (see details in App.E).

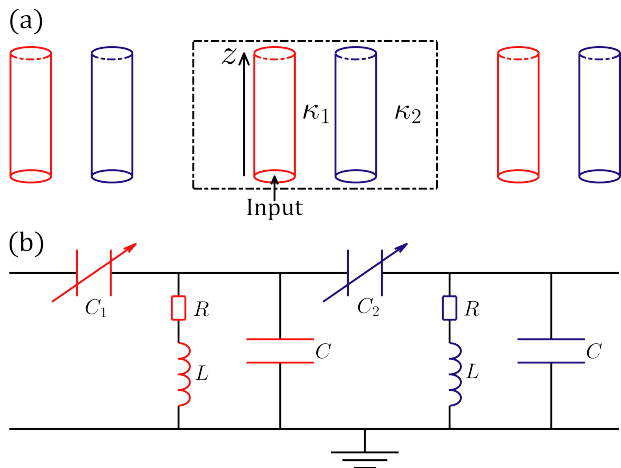


FIG. 4. Experimental proposals for nonlinear topological systems. (a) 1D array of nonlinear optic lattice. (b) The unit cell of nonlinear topoelectrical circuit.

Topological photonics[45, 46]: Our theoretical prototype is readily testified in 1D array of optic lattice. Each unit cell is composed of two waveguides to guide modes along the axial direction, and the nearest neighbors are coupled by nonlinear overlap of adjacent electric fields[46]. The modes are described by Eqs.(1), and the

system meets all requirements to realize topological properties in fully nonlinear regime.

Topoelectrical circuit[8]: A second promising direction is to construct a ladder of cascaded diatomic unit cells composed of two LC resonators and two small nonlinear capacitors $C_{i=1,2}(V) \ll C$. The motion equation of the unit cell voltages $V_n^{(i=1,2)}$ are captured by Eqs.(1), where the couplings are nonlinear functions of voltages. Topological attributes in fully nonlinear regime can be studied in this model.

V. CONCLUSIONS

In this paper, we extend topological band theory to fully nonlinear regime where nonlinear bulk modes are remarkably different from sinusoidal waves. The proper definition of Berry phase is carried out for nonlinear bulk modes, and its quantization is demonstrated in reflection-symmetric models. This topological invariant experiences an interesting transition induced by bulk mode amplitudes. The advent and disappearance of topological boundary modes demonstrate the nonlinear extension of bulk-edge correspondence.

A rich variety of problems can be studied following this work, such as the nonlinear extension of Chern number and chiral edge modes in 2D systems[1]. Another intriguing direction is to discover higher-order topological states[47] in nonlinear systems. Finally, it would be challenging to study how topological phases influence other nonlinear properties, such as instability, bifurcation, and chaos.

ACKNOWLEDGMENTS

D. Z. would like to thank insightful discussions with Xueda Wen, Junyi Zhang, D. Zeb Rocklin, and Michael Leamy.

Appendix A: Berry phase of nonlinear bulk modes

In this section, we derive Berry phase of nonlinear bulk modes by adiabatically evolving the wave function as the wavenumber q slowly traverses the Brillouin zone. We consider the nonlinear problem described by a classical two-field generalized nonlinear Schrödinger equations presented in the main text,

$$\begin{aligned} i\partial_t \Psi_n^{(1)} &= \epsilon_0 \Psi_n^{(1)} + f_1(\Psi_n^{(1)}, \Psi_n^{(2)}) + f_2(\Psi_n^{(1)}, \Psi_{n-1}^{(2)}), \\ i\partial_t \Psi_n^{(2)} &= \epsilon_0 \Psi_n^{(2)} + f_1(\Psi_n^{(2)}, \Psi_n^{(1)}) + f_2(\Psi_n^{(2)}, \Psi_{n+1}^{(1)}), \end{aligned} \quad (\text{A1})$$

where $f_i(x, y)$ for $i = 1, 2$ are real-coefficient general polynomials of x, x^*, y , and y^* . Berry phase is derived from this general model.

In the linear limit, the interactions are approximated as $f_i(x, y) \approx c_i y$ ($c_{i=1,2} > 0$). The model is a 2×2

matrix problem in which the bands are gapped. As the amplitude rises, nonlinearities become increasingly significant and the linear bulk modes evolve into nonlinear bulk modes. In this section, we study the simple case that the nonlinear bulk modes are non-degenerate and are stable. In other words, a nonlinear bulk mode is unique, provided that the amplitude A , the frequency ω , and the wavenumber q are given. In addition to these properties, we consider the simple case that the nonlinear bandgap[8, 19] never closes. As such, this system is a nonlinear extension of the linear two-band model.

We begin by defining the nonlinear periodic bulk mode of the system as follows,

$$\Psi_n(t) = \Psi_q(\omega t - nq) = \begin{pmatrix} \Psi_q^{(1)}(\omega t - nq) \\ \Psi_q^{(2)}(\omega t - nq + \phi_q) \end{pmatrix}, \quad (\text{A2})$$

where q is the wavenumber and ω is the eigenfrequency that belongs to the upper band of the nonlinear band structure. In general, the waveforms of $\Psi_q^{(j)}(\theta)$ for $j = 1, 2$ are not sinusoidal in θ . We note that because the wave function component $\Psi_q^{(j)}(\theta)$ is 2π -periodic, it is defined up to an arbitrary phase condition. In this paper, the phase condition is chosen by asking that when $\theta = 0$, the real part of wave component $\text{Re} \Psi_q^{(j)}(\theta)$ reaches its amplitude/maximum,

$$\text{Re} \Psi_q^{(j)}(\theta = 0) = \max(\text{Re} \Psi_q^{(j)}(\theta)) \stackrel{\text{def}}{=} A, \quad j = 1, 2. \quad (\text{A3})$$

We note that the phase condition in Eq.(A3) is similar to that in exponential functions, where $\text{Re} e^{i\theta=0} = \max(\text{Re} e^{i\theta})$. Following this convention, ϕ_q in Eq.(A2) characterizes the relative phase between $\Psi_q^{(1)}$ and $\Psi_q^{(2)}$. The nonlinear mode has to fulfill the differential equation parametrized by wavenumber q ,

$$i\partial_t \Psi_q(\theta) = H(\Psi_q), \quad (\text{A4})$$

where $\theta = \omega t$, and the nonlinear function $H(\Psi_q)$ is given by

$$\begin{aligned} H(\Psi_q) = & \begin{pmatrix} \epsilon_0 \Psi_q^{(1)}(\theta) \\ \epsilon_0 \Psi_q^{(2)}(\theta + \phi_q) \end{pmatrix} \\ & + \begin{pmatrix} f_1(\Psi_q^{(1)}(\theta), \Psi_q^{(2)}(\theta + \phi_q)) \\ f_1(\Psi_q^{(2)}(\theta + \phi_q), \Psi_q^{(1)}(\theta)) \end{pmatrix} \\ & + \begin{pmatrix} f_2(\Psi_q^{(1)}(\theta), \Psi_q^{(2)}(\theta + q + \phi_q)) \\ f_2(\Psi_q^{(2)}(\theta + \phi_q), \Psi_q^{(1)}(\theta - q)) \end{pmatrix}. \end{aligned} \quad (\text{A5})$$

In what follows, we study the nonlinear bulk mode with the fixed amplitude A . Therefore, the mode frequency ω , the relative phase ϕ_q , and the waveform are controlled by the wavenumber q .

Next, we adiabatically evolve the wavenumber $q(t)$ traversing the Brillouin zone from $q(0) = q$ to $q(t) = q + 2\pi$. According to the nonlinear extension of adiabatic theorem[37–40], a system initially in one of its nonlinear eigenmode Ψ_q of the upper band will stay as an instantaneous upper-band nonlinear eigenmode of $H(\Psi_{q(t)})$

throughout the process. This theorem is valid when the control parameter q varies sufficiently slowly compared to the frequencies[38], and the nonlinear bulk modes are stable[39] within the amplitude scope of this paper. In App.C, we exploit the self-oscillation method[36] to confirm the stability of these nonlinear modes. Hence the only degree of freedom is the phase of the eigenmode. At time t , the eigenmode Ψ is

$$\Psi = \Psi_{q(t)} \left(\int_0^t \omega(t', q(t')) dt' - \gamma(t) \right). \quad (\text{A6})$$

We are interested in the extra phase term γ , which will be carried out as follows. Substituting Eq.(A6) into Eq.(A4), we have

$$\frac{d\gamma}{dt} \frac{\partial \Psi_q}{\partial \theta} = \frac{dq}{dt} \frac{\partial \Psi_q}{\partial q}, \quad (\text{A7})$$

where $\theta = \omega t$ stands for the phase of the wave function Ψ_q . We bare in mind that the nonlinear bulk mode is 2π -periodic in its phase, which grants Fourier transformation. We expand $\Psi_q^{(j)}(\theta)$, the component of periodic wave function, in terms of its Fourier series:

$$\Psi_q^{(j)}(\theta) = \sum_{l \in \mathcal{Z}} \psi_{l,q}^{(j)} e^{-il\theta} \quad j = 1, 2, \quad (\text{A8})$$

where $\psi_{l,q}^{(j)}$ is the l -th Fourier component of $\Psi_q^{(j)}$ (l is integer). Inserting Eq.(A8) into Eq.(A7), we have

$$\begin{aligned} \frac{d\gamma}{dt} \sum_l i l e^{-il\theta} \begin{pmatrix} \psi_{l,q}^{(1)} \\ \psi_{l,q}^{(2)} e^{-il\phi_q} \end{pmatrix} = \\ - \frac{dq}{dt} \sum_l e^{-il\theta} \begin{pmatrix} \partial \psi_{l,q}^{(1)} / \partial q \\ e^{-il\phi_q} [\partial \psi_{l,q}^{(2)} / \partial q - il \psi_{l,q}^{(2)} (\partial \phi_q / \partial q)] \end{pmatrix}. \end{aligned} \quad (\text{A9})$$

We multiply Eq.(A9) on both sides by $\Psi_q^\dagger(\theta)$ and integrate θ from 0 to 2π , to obtain the following result,

$$\begin{aligned} \frac{d\gamma}{dt} \sum_{l'} i l' (|\psi_{l',q}^{(1)}|^2 + |\psi_{l',q}^{(2)}|^2) = \\ \frac{dq}{dt} \sum_l \left(i l |\psi_{l,q}^{(2)}|^2 \frac{\partial \phi_q}{\partial q} - \psi_{l,q}^{(1)*} \frac{\partial \psi_{l,q}^{(1)}}{\partial q} - \psi_{l,q}^{(2)*} \frac{\partial \psi_{l,q}^{(2)}}{\partial q} \right). \end{aligned} \quad (\text{A10})$$

Since the wavenumber q traverses the Brillouin zone, by integrating over time t we obtain the phase term γ expressed in terms of a loop integration through the entire Brillouin zone,

$$\gamma = \oint_{\text{BZ}} dq \frac{\sum_l \left(l |\psi_{l,q}^{(2)}|^2 \frac{\partial \phi_q}{\partial q} + i \sum_j \psi_{l,q}^{(j)*} \frac{\partial \psi_{l,q}^{(j)}}{\partial q} \right)}{\sum_{l'} l' (|\psi_{l',q}^{(1)}|^2)}. \quad (\text{A11})$$

Eq.(A11) is Berry phase of the upper-band nonlinear bulk modes, which is the generalization of Berry phase in linear problems. We note that in quantum mechanics, Schrödinger equation is linear and the eigenmodes are sinusoidal in time. As a result, Fourier component $\psi_{l,q}^{(j)}$ in Schrödinger equation only appears in $l = 1$ or -1 , and Berry phase in Eq.(A11) reduces to the conventional form, $\gamma = \oint_{\text{BZ}} dq i \langle \Psi_q | \partial_q | \Psi_q \rangle$.

Appendix B: Symmetries of generalized nonlinear Schrödinger equations and the quantization of Berry phase

In this section, we study symmetry properties of the model in Eqs.(A1) and demonstrate the quantization of Berry phase in Eq.(A11).

1. Reflection symmetry and quantized Berry phase

Before going into details of reflection symmetry in the nonlinear system, we briefly review this symmetry in the linearized model and demonstrate the quantization of Berry phase, when the coupling is linearized as $f_i(x, y) = c_i y$. We convert the wave function into momentum space $\Psi_n = \Psi_q e^{i(qn - \omega t)}$, to reduce the equations of motion as $H_q \Psi_q = \omega \Psi_q$, where $H_q = \epsilon_0 I + (c_1 + c_2 \cos q) \sigma_x + (c_2 \sin q) \sigma_y$, and $\sigma_{x,y,z}$ are Pauli matrices. H_q is subjected to reflection symmetry, meaning that one can find a reflection symmetry operator $M_x = \sigma_x$, such that $M_x^2 = I$, and $M_x H_q M_x^{-1} = H_{-q}$. We notice $H_{-q} M_x \Psi_q = \omega M_x \Psi_q$. It demonstrates that Ψ_q and Ψ_{-q} are related by $M_x \Psi_q = e^{i\phi_q} \Psi_{-q}$, where ϕ_q is the phase factor connecting Ψ_q and Ψ_{-q} . At high-symmetry points when $q_{\text{hs}} = 0, \pi$ ("hs" is short for high symmetry), we find that M_x and H_q commute, which demands the phase factor $\phi_{\text{hs}} = 0$ or π . Finally, in the linear problem, we prove the quantization of Berry phase by showing that $\gamma = \phi_\pi - \phi_0 = 0$ or $\pi \pmod{2\pi}$.

We now proceed to investigate the nonlinear problem raised in Eqs.(A1). We denote the periodic nonlinear bulk mode as

$$\Psi_q = (\Psi_q^{(1)}(\omega t - qn), \Psi_q^{(2)}(\omega t - qn + \phi_q))^\top, \quad (\text{B1})$$

where the frequency ω lies in the upper-band of the nonlinear band structure, and q is the wavenumber. Ψ_q is a solution of Eqs.(A1) only if it fulfills Eq.(A4), which is equivalent to the following nonlinear differential equation,

$$\begin{aligned} \Psi_q(\theta = \omega t - qn) &= (\Psi_q^{(1)}(\theta), \Psi_q^{(2)}(\theta + \phi_q))^\top : \\ \mathcal{L}(\Psi_q) &= 0, \end{aligned} \quad (\text{B2})$$

where the nonlinear differential operator $\mathcal{L}(\Psi_q)$ is defined as follows,

$$\begin{aligned} \mathcal{L}(\Psi_q) &= (i\omega \partial_\theta - \epsilon_0) \begin{pmatrix} \Psi_q^{(1)}(\theta) \\ \Psi_q^{(2)}(\theta) \end{pmatrix} \\ &\quad - \begin{pmatrix} f_1(\Psi_q^{(1)}(\theta), \Psi_q^{(2)}(\theta + \phi_q)) \\ f_1(\Psi_q^{(2)}(\theta), \Psi_q^{(1)}(\theta - \phi_q)) \end{pmatrix} \\ &\quad - \begin{pmatrix} f_2(\Psi_q^{(1)}(\theta), \Psi_q^{(2)}(\theta + q + \phi_q)) \\ f_2(\Psi_q^{(2)}(\theta), \Psi_q^{(1)}(\theta - q - \phi_q)) \end{pmatrix}. \end{aligned} \quad (\text{B3})$$

In general, the waveform of Ψ_q is not sinusoidal, which is the natural result of nonlinearity. Following the notation

of Eq.(B1), the nonlinear bulk mode of frequency ω and wavenumber $-q$ is denoted as

$$\Psi_{-q}(\theta = \omega t + qn) = (\Psi_{-q}^{(1)}(\theta), \Psi_{-q}^{(2)}(\theta + \phi_{-q}))^\top. \quad (\text{B4})$$

Next, we notice that the nonlinear system is subjected to reflection symmetry: the equations of motion are invariant under the reflection transformation,

$$(\Psi_n^{(1)}, \Psi_n^{(2)}) \rightarrow (\Psi_{-n}^{(2)}, \Psi_{-n}^{(1)}). \quad (\text{B5})$$

Given a nonlinear bulk mode solution Ψ_q that renders $\mathcal{L}(\Psi_q)$ to vanish, Eq.(B5) demands a new nonlinear bulk mode solution $\Psi'_{-q} = (\Psi_q^{(2)}(\omega t + qn), \Psi_q^{(1)}(\omega t + qn - \phi_q))^\top$ that also renders $\mathcal{L}(\Psi'_{-q})$ to vanish,

$$\begin{aligned} \Psi'_{-q}(\theta = \omega t + qn) &= (\Psi_q^{(2)}(\theta), \Psi_q^{(1)}(\theta - \phi_q))^\top : \\ \mathcal{L}(\Psi'_{-q}) &= \sigma_x \mathcal{L}(\Psi_q) = 0. \end{aligned} \quad (\text{B6})$$

It is obvious that Ψ'_{-q} is a nonlinear solution with the frequency ω and wavenumber $-q$. Due to the non-degenerate nature of the nonlinear bulk modes, Ψ_{-q} and Ψ'_{-q} have to be the same solution, which in turn imposes the constraints

$$\Psi_{-q}^{(1)}(\theta) = \Psi_q^{(2)}(\theta), \quad (\text{B7})$$

and

$$-\phi_q = \phi_{-q} \pmod{2\pi}. \quad (\text{B8})$$

Having obtained Eqs.(B7, B8), we now attempt to prove the quantization of Berry phase defined in Eq.(A11). To this end, we consider the Fourier components of $\Psi_q^{(1)}$ and $\Psi_q^{(2)}$, which are related to one another as follows,

$$\psi_{l,-q}^{(1)} = \psi_{l,q}^{(2)}. \quad (\text{B9})$$

Employing Eq.(B8) and Eq.(B9), we compute Berry phase by separating it into two parts, $\gamma = \gamma_1 + \gamma_2$, where

$$\gamma_1 = i \oint_{\text{BZ}} dq \frac{\sum_l \left(\psi_{l,q}^{(1)*} \frac{\partial \psi_{l,q}^{(1)}}{\partial q} + \psi_{l,-q}^{(1)*} \frac{\partial \psi_{l,-q}^{(1)}}{\partial q} \right)}{\sum_{l'} l' \left(|\psi_{l',q}^{(1)}|^2 + |\psi_{l',-q}^{(1)}|^2 \right)} = 0, \quad (\text{B10})$$

and

$$\begin{aligned} \gamma_2 &= \frac{1}{2} \oint_{\text{BZ}} dq \frac{\sum_l l \left(|\psi_{l,q}^{(1)}|^2 + |\psi_{l,-q}^{(1)}|^2 \right)}{\sum_{l'} l' \left(|\psi_{l',q}^{(1)}|^2 + |\psi_{l',-q}^{(1)}|^2 \right)} \frac{\partial \phi_q}{\partial q} \\ &= \frac{1}{2} \oint_{\text{BZ}} dq \frac{\partial \phi_q}{\partial q} = \phi_\pi - \phi_0. \end{aligned} \quad (\text{B11})$$

Next, at high-symmetry points $q_{\text{hs}} = 0, \pi$, we find that $\phi_{q_{\text{hs}}} = \phi_{-q_{\text{hs}}}$. Together with Eq.(B8), we obtain $2\phi_{\text{hs}} = 0 \pmod{2\pi}$, meaning that

$$\phi_\pi - \phi_0 = 0 \text{ or } \pi \pmod{2\pi}. \quad (\text{B12})$$

Therefore, we demonstrate the quantization of Berry phase,

$$\gamma = 0 \text{ or } \pi \pmod{2\pi}. \quad (\text{B13})$$

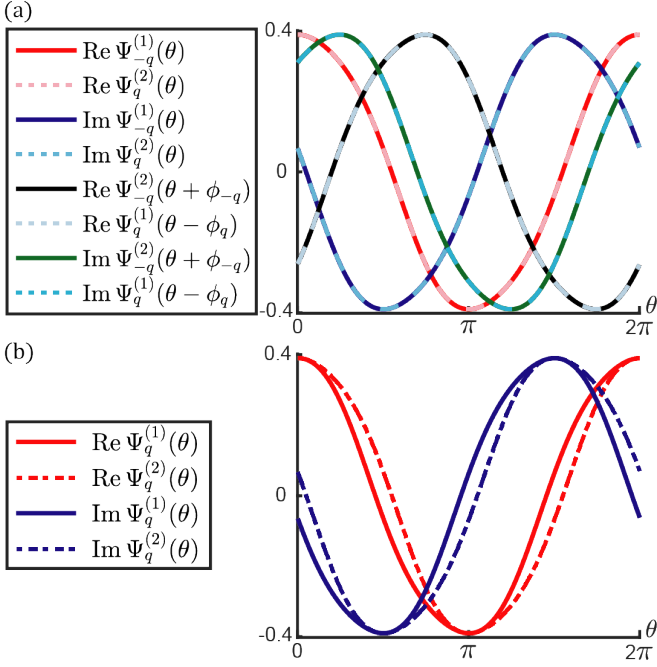


FIG. 5. Numerical verification of $\Psi_{-q}^{(1)}(\theta) = \Psi_{-q}^{(2)}(\theta)$ and $-\phi_q = \phi_{-q}$ by computing nonlinear bulk modes. Here the nonlinear bulk modes are calculated in the lattice composed of classical dimer fields. The lattice is subjected to periodic boundary condition (PBC), and the interaction parameters are carried over from fig.3, where $\epsilon_0 = 0$, $c_1 = 0.25$, $c_2 = 0.37$, $d_1 = 0.22$, and $d_2 = 0.02$. (a) Numerical illustration of Eqs.(B7, B8) by comparing nonlinear bulk modes $\Psi_{-q}(t)$ in Eq.(B4) and $\Psi'_{-q}(t)$ in Eq.(B6), where the wavenumber $q = 8\pi/9$ and the amplitude $A = 0.3873$. $\Psi_{-q}^{(1)}(\theta) = \Psi_{-q}^{(2)}(\theta)$ and $-\phi_q = \phi_{-q}$ are verified by the perfect overlap between the wave functions. (b) Numerical demonstration of $\text{Re } \Psi_q^{(1)}(\theta) \neq \text{Re } \Psi_q^{(2)}(\theta)$ and $\text{Im } \Psi_q^{(1)}(\theta) \neq \text{Im } \Psi_q^{(2)}(\theta)$.

2. Additional properties when the nonlinear interactions yield $f_i(-x, y) = -f_i(x, -y)$

In the minimal model, the functional forms of nonlinear interactions yield $f_i(-x, y) = -f_i(x, -y)$ (or equivalently, $f_i(-x, -y) = -f_i(x, y)$). Given a nonlinear bulk mode Ψ_q , it is straightforward to prove that $-\Psi_q$ is a nonlinear solution as well. Hence, Ψ_q and $-\Psi_q$ must differ by a phase $\Delta\theta$ only, such that $\Psi_q(\theta + \Delta\theta) = -\Psi_q(\theta)$. We perform the phase shift $\Delta\theta$ twice to have $\Psi_q(\theta + 2\Delta\theta) = \Psi_q(\theta)$, which imposes $\Delta\theta = \pi$. Finally, we reach the conclusion

$$\Psi_q(\theta + \pi) = -\Psi_q(\theta). \quad (\text{B14})$$

3. Symmetry properties of nonlinear bulk modes when $\epsilon_0 = 0$

When $\epsilon_0 = 0$, the linearized model of Eqs.(A1) is subjected to an additional symmetry called charge-conjugation symmetry[5, 6]. In the small-amplitude

limit, the interactions are reduced to $f_i(\Psi_n^{(j)}) = c_i \Psi_n^{(j)}$. We convert wave function to momentum space $\Psi_n^{(j)} = \Psi_\omega^{(j)} e^{i(qn - \omega t)}$ to have the reduced equation of motion, $H\Psi_\omega = \omega\Psi_\omega$, where $H = (c_1 + c_2 \cos q)\sigma_x + (c_2 \sin q)\sigma_y$. H is subjected to charge-conjugation symmetry, meaning that one can find a symmetry operator $\Pi = \sigma_z$ such that $\Pi^2 = I$, and $\Pi H \Pi^{-1} = -H$. As a result, $H\Pi\Psi_\omega = -\omega\Pi\Psi_\omega$, meaning that the eigenvalues always come in $\pm\omega$ pairs, and the eigenmodes Ψ_ω , $\Psi_{-\omega}$ are related by $\Pi\Psi_\omega = e^{i\phi_q}\Psi_{-\omega}$. This relationship demonstrates the quantization of Berry phase when we evaluate it in the upper band.

We then study the nonlinear model in Eqs.(A1) with $\epsilon_0 = 0$ and the associated nonlinear modes. In order to have the eigenfrequencies of nonlinear modes to appear in $\pm\omega$ pairs, we ask that the nonlinear interactions $f_i(x, y)$ to yield the following constraints:

$$f_i(-x, y) = -f_i(x, -y) = f_i(x, y), \quad (\text{B15})$$

for $i = 1, 2$. In linear systems, $f_i(x, y)$ is reduced to $f_i(x, y) = c_i y$ and this property is naturally met. However, this property is not naturally satisfied by arbitrary nonlinear functions, and Eqs.(B15) are the additional constraints for nonlinear interactions. As a result, the system is invariant under the transformation

$$(\Psi_n^{(1)}(\omega t), \Psi_n^{(2)}(\omega t)) \rightarrow (-\Psi_n^{(1)}(-\omega t), \Psi_n^{(2)}(-\omega t)). \quad (\text{B16})$$

Let us consider a nonlinear bulk mode solution Ψ_ω of the upper band with the frequency $\omega > 0$ and wavenumber q . It yields the following nonlinear differential equation,

$$\begin{aligned} \Psi_\omega(\theta = \omega t - qn) &= (\Psi_q^{(1)}(\theta), \Psi_q^{(2)}(\theta + \phi_q))^\top : \\ \mathcal{L}(\Psi_\omega; \epsilon_0 = 0) &= 0. \end{aligned} \quad (\text{B17})$$

Referring to Eq.(B16), it is straightforward to find a ‘‘partner solution $\Psi_{-\omega}$ ’’ of frequency $-\omega < 0$ and wavenumber q , that satisfies the nonlinear differential equation,

$$\begin{aligned} \Psi_{-\omega}(\theta = -\omega t - qn) &= (-\Psi_q^{(1)}(\theta), \Psi_q^{(2)}(\theta + \phi_q))^\top : \\ \mathcal{L}(\Psi_{-\omega}; \epsilon_0 = 0) &= \sigma_z \mathcal{L}(\Psi_\omega; \epsilon_0 = 0) = 0. \end{aligned} \quad (\text{B18})$$

Eq.(B18) demonstrates that the eigenfrequencies of nonlinear bulk modes always appear in $\pm\omega$ pairs. Consequently, $\Psi_{-\omega}$ is the nonlinear bulk mode solution that belongs to the lower band, and the nonlinear band structure is symmetric with respect to $\omega = 0$ axis.

Appendix C: Methods of computing nonlinear bulk modes

In this section, we introduce the methods of computing nonlinear bulk modes, which are commonly used in solving nonlinear problems. We illustrate these methods by considering the model of Eqs.(A1) with the nonlinear interactions specified in Eq.(11) of the main text,

$$f_i(x, y) = c_i y + d_i [(\text{Re } y)^3 + i(\text{Im } y)^3]. \quad (\text{C1})$$

In the weakly nonlinear regime, the analytic and perturbative *method of multiple-scale*[33, 34, 36] finds nonlinear bulk modes asymptotically, which serves as the cornerstone of nonlinear modes for higher amplitudes. As the amplitude grows, the system enters into a region where this perturbative technique is unavailable. Instead, the numerical tactic called *shooting method*[41–43] finds nonlinear bulk modes for large amplitudes, and these modes are noticeably different from sinusoidal waves (figs.1(b), 3(b), and 3(d)). In this paper, we combine these two methods, i.e., method of multiple-scale and shooting method, to obtain a series of nonlinear bulk modes for a wide range of amplitudes.

1. Method of multiple-scale: bulk modes in weakly nonlinear regime

First of all, we explore bulk modes in the weakly nonlinear regime. The perturbative approach, namely method of multiple-scale, is useful to solve the eigenfrequencies and waveforms of weakly nonlinear bulk modes.

This method is performed by introducing a small book-keeping parameter $\epsilon \ll 1$ that enforces small amplitudes for the bulk modes. Specifically, this parameter is introduced by rewriting d_i as ϵd_i in Eq.(C1). This method then expands the time derivatives in orders of slow-time derivatives,

$$\frac{d}{dt} = \sum_{l=0}^{\infty} \epsilon^l D_l, \quad (\text{C2})$$

where $T_{(l)} = \epsilon^l T_{(0)}$ is the l -th order slow time variable, and $D_l = \partial/\partial T_{(l)}$ is the corresponding slow time deriva-

tive. Next, the wave function is also expanded in terms of the multiple-scale,

$$\Psi_n = \sum_{l=0}^{\infty} \epsilon^l \Psi_{n,(l)}, \quad (\text{C3})$$

where $\Psi_{n,(l)} = (\Psi_{n,(l)}^{(1)}, \Psi_{n,(l)}^{(2)})^\top$ is the l -th order wave function. In what follows, we calculate $\Psi_{n,(l=1)}$, which offers us the wave function correction and the frequency correction of the first order. Following Eqs.(C2, C3), we expand the equations of motion by matching all field variables with respect to the order of the book-keeping parameter ϵ . To zeroth-order, the equations of motion are given as

$$L(\Psi_{n,(0)}) = 0, \quad (\text{C4})$$

where the Linear operator $L(\Psi_n)$ is specified below,

$$L(\Psi_n) = \begin{pmatrix} iD_0 \Psi_n^{(1)} - \epsilon_0 \Psi_n^{(1)} - c_1 \Psi_n^{(2)} - c_2 \Psi_{n-1}^{(2)} \\ iD_0 \Psi_n^{(2)} - \epsilon_0 \Psi_n^{(2)} - c_1 \Psi_n^{(1)} - c_2 \Psi_{n+1}^{(1)} \end{pmatrix}. \quad (\text{C5})$$

The solution to the zeroth-order equations is

$\Psi_{n,(0)} = iA(T_{(1)})e^{iqn - i\omega_{(0)}T_{(0)} - i\theta(T_{(1)})} (e^{i\phi_q^{(0)}}, 1)^\top$, (C6) where $\Delta\omega_{(0)} = \omega_{(0)} - \epsilon_0 = \pm\sqrt{c_1^2 + c_2^2 + 2c_1c_2 \cos q}$, $\tan \phi_q^{(0)} = -c_2 \sin q / (c_1 + c_2 \cos q)$, and $\theta = \theta(T_{(1)})$ is the arbitrary phase condition for the bulk modes. We note that this phase is a constant up to the fast time scale $T_{(0)}$ but can depend on the slow time scale $T_{(1)}$. It provides the frequency shift due to the nonlinearities. In what follows, we will focus on computing this frequency shift. To this end, we consider the first-order equations of motion,

$$L(\Psi_{n,(1)}) + \begin{pmatrix} iD_1 \Psi_{n,(0)}^{(1)} - d_1 [(\text{Re } \Psi_{n,(0)}^{(2)})^3 + i(\text{Im } \Psi_{n,(0)}^{(2)})^3] - d_2 [(\text{Re } \Psi_{n-1,(0)}^{(2)})^3 + i(\text{Im } \Psi_{n-1,(0)}^{(2)})^3] \\ iD_1 \Psi_{n,(0)}^{(2)} - d_1 [(\text{Re } \Psi_{n,(0)}^{(1)})^3 + i(\text{Im } \Psi_{n,(0)}^{(1)})^3] - d_2 [(\text{Re } \Psi_{n+1,(0)}^{(1)})^3 + i(\text{Im } \Psi_{n+1,(0)}^{(1)})^3] \end{pmatrix} = 0. \quad (\text{C7})$$

The solution of Eq.(C7), namely the first-order correction of wave function $\Psi_{n,(1)}$, has two components $\Psi_{n,(1)} = \Psi_{n,(1)}(\omega) + \Psi_{n,(1)}(3\omega)$: a fundamental-harmonic part $\Psi_{n,(1)}(\omega)$ and a third-harmonic part $\Psi_{n,(1)}(3\omega)$. We are interested in how the nonlinearities modify the eigenfrequencies of the bulk modes, which stem from the secular term generated by the fundamental harmonics. On the other hand, the frequency-tripling part does not contribute to the secular term and the subsequent frequency shift. Hence, we consider the fundamental harmonic part only. The equations of the fundamental part $\Psi_{n,(1)}(\omega)$ is given as follows,

$$L(\Psi_{n,(1)}(\omega)) + e^{i(qn - \omega_{(0)}T_{(0)} - \theta)} \begin{pmatrix} (-D_1 A + iAD_1\theta)e^{i\phi_q^{(0)}} - \frac{3}{4}iA^3(d_1 + d_2e^{-iq}) \\ (-D_1 A + iAD_1\theta) - \frac{3}{4}iA^3(d_1 + d_2e^{iq})e^{i\phi_q^{(0)}} \end{pmatrix} = 0. \quad (\text{C8})$$

We want to find $\Psi_{n,(1)}(\omega)$ orthogonal to $\ker(L(\Psi_n))$, which is of the form

$$\Psi_{n,(1)}(\omega) = a(e^{i\phi_q^{(0)}}, -1)^\top e^{i(qn - \omega_0 T_{(0)} - \theta(T_{(1)}))}, \quad (\text{C9})$$

where a is a complex number. We use Eq.(C8) to solve

a , $D_1 A$, and $D_1 \theta$,

$$\begin{aligned} D_1 \theta &= \frac{3A^2}{4} [d_1 \cos \phi_q^{(0)} + d_2 \cos(\phi_q^{(0)} + q)], \\ D_1 A &= 0, \\ a &= \frac{3A^3}{8\Delta\omega_{(0)}} [d_1 \sin \phi_q^{(0)} + d_2 \sin(\phi_q^{(0)} + q)]. \end{aligned} \quad (\text{C10})$$

We note that the result $D_1 A = 0$ is natural for undamped systems. In Eqs.(C10), since $a \in \mathcal{R}$ is real, it is convenient to denote the real quantity $\phi_q^{(1)} = -2a/A$. To the order $\mathcal{O}(\epsilon^1)$, the bulk mode solution can therefore be simplified as the following compact form,

$$\Psi_n = iA(e^{i(\phi_q^{(0)} + \frac{1}{2}\epsilon\phi_q^{(1)})}, e^{-\frac{1}{2}i\epsilon\phi_q^{(1)}})^\top e^{iqn - i(\omega_{(0)} + \epsilon D_1 \theta)T_{(0)}}. \quad (\text{C11})$$

Hence, as the amplitude rises, the relative phase between two wave components changes from $\phi_q^{(0)}$ to $\phi_q^{(0)} + \epsilon\phi_q^{(1)}$.

Method of multiple-scale is a trustworthy technique in weakly nonlinear regime by allowing perturbative analysis. It provides nonlinear effects quantitatively, like the frequency shift $D_1 \theta$. They help to verify the correctness of other numerical methods in fully nonlinear regime. The good agreement of the frequency shift in weakly nonlinear regime between method of multiple-scale and shooting method is presented in fig.6.

2. Shooting method: bulk modes in fully nonlinear regime

Secondly, we introduce shooting method which numerically computes nonlinear bulk modes of Eqs.(A1) in fully nonlinear regime, where the nonlinearities are comparable to the linear interactions and perturbation theory breaks down. We define the $4N \times 1$ vector field $z(t)$ which describes the wave functions of all particles,

$$z(t) = (\text{Re } \Psi_1^{(1)}, \text{Im } \Psi_1^{(1)}, \text{Re } \Psi_1^{(2)}, \text{Im } \Psi_1^{(2)}, \dots, \text{Re } \Psi_N^{(1)}, \text{Im } \Psi_N^{(1)}, \text{Re } \Psi_N^{(2)}, \text{Im } \Psi_N^{(2)})^\top. \quad (\text{C12})$$

The equation of motion for $z(t)$ is $dz/dt = g(z)$, which in turn gives

$$z(t) = z(0) + \int_0^t g(z(t'))dt', \quad (\text{C13})$$

where $g(z)$ is a $4N \times 1$ vector derived from the nonlinear equations of motion. Each component is displayed as follows,

$$\begin{aligned} g_{4n-3} &= +\epsilon_0 z_{4n-2} + F_1(z_{4n-0}) + F_2(z_{4n-4}), \\ g_{4n-2} &= -\epsilon_0 z_{4n-3} - F_1(z_{4n-1}) - F_2(z_{4n-5}), \\ g_{4n-1} &= +\epsilon_0 z_{4n-0} + F_1(z_{4n-2}) + F_2(z_{4n+2}), \\ g_{4n-0} &= -\epsilon_0 z_{4n-1} - F_1(z_{4n-3}) - F_2(z_{4n+1}), \end{aligned} \quad (\text{C14})$$

where $1 \leq n \leq N$, and $F_i(x) = c_i x + d_i x^3$.

The considered nonlinear wave function at time $t = 0$ reads $z(t = 0)$. It evolves forward in time for T , and then the wave function is given by $z(t = T)$. In general, $z(T) \neq z(0)$ since the considered wave may not be periodic in time. In the rest of this section, we denote the nonlinear mode that starts with $z(0)$ and evolves forward in time for T as $\{z(0), T\}$. We further denote a periodic nonlinear solution as $\{z_p(0), T_p\}$, meaning that at $t = 0$

the wave function is $z_p(t = 0)$ and the mode period is T_p . Thus, it is straightforward to have $z_p(T_p) - z_p(0) = 0$. In order to quantify ‘‘how far away’’ $\{z(0), T\}$ is from $\{z_p(0), T_p\}$, we define the ‘‘shooting function’’ $H(z(0), T)$ as follows,

$$H(z(0), T) = z(T) - z(0) = \int_0^T g(z(t))dt. \quad (\text{C15})$$

$H(z(0), T) \neq 0$ for a temporal aperiodic mode $\{z(0), T\}$, and $H(z_p(0), T_p) = 0$ for the periodic solution $\{z_p(0), T_p\}$. The smaller the shooting function $H(z(0), T)$ is, the closer $\{z(0), T\}$ is to the periodic solution.

From now on we attempt to find periodic solutions by lowering the shooting function in a recursive algorithm, which is known as shooting method. We start the algorithm with a guessing initial wave function $\{z_1(0), T_1\}$: at $t = 0$, the imported guessing wave is $z_1(t = 0)$ and the imported guessing period is T_1 , which means we will evolve $z_1(t = 0)$ forward in time for T_1 to evaluate the shooting function $H(z_1(0), T_1)$. Here, $z_1(t = 0)$ and $T_1 = 2\pi/(\omega_{(0)} + \epsilon D_1 \theta)$ are chosen from Eq.(C11), which implicitly determines the wavenumber q . $\{z_1(0), T_1\}$ is not a true periodic solution, and the subsequent shooting function $H(z_1(0), T_1) \neq 0$. In order to approach the true periodic solution $\{z_p(0), T_p\}$, we make corrections to $\{z_1(0), T_1\}$ to obtain the second guessing solution $\{z_2(0), T_2\}$. We repeat this process to obtain a series of guessing solutions $\{z_l(0), T_l\}$ ($l \geq 1$). The corresponding shooting functions $H(z_l(0), T_l)$ slowly converge to zero as l increases.

In the l -th step, the guessing solution is denoted as $\{z_l(0), T_l\}$, and the associated shooting function is $H(z_l(0), T_l) \neq 0$. Therefore, we make corrections $\{\Delta z_l(0), \Delta T_l\}$ to the l -th step guessing solution to obtain the guessing solution of $(l + 1)$ -th step,

$$\{z_{l+1}(0), T_{l+1}\} = \{z_l(0) + \eta_A^{-1} \Delta z_l(0), T_l + \eta_T^{-1} \Delta T_l\}, \quad (\text{C16})$$

such that

$$|H(z_{l+1}(0), T_{l+1})| < |H(z_l(0), T_l)|. \quad (\text{C17})$$

In other words, $H(z_{l+1}(0), T_{l+1})$ is closer to zero than $H(z_l(0), T_l)$. η_A and η_T in Eq.(C16) are constants greater than 1, which slow down the evolution speed. In order to achieve Eq.(C17), the correction $\{\Delta z_l(0), \Delta T_l\}$ is determined by the following matrix equation,

$$\begin{aligned} H(z_{l+1}(0), T_{l+1}) &\approx \\ H(z_l(0), T_l) + \frac{\partial H}{\partial z_l(0)} \Delta z_l(0) + \frac{\partial H}{\partial T_l} \Delta T_l &= 0, \end{aligned} \quad (\text{C18})$$

where the matrices $\partial H/\partial z_l(0)$ and $\partial H/\partial T_l$ will be elaborated later. By repeating the above process, we generate a sequence of guessing solutions $\{z_l(0), T_l\}$, from which the shooting functions converge to zero,

$$\begin{aligned} \lim_{l \rightarrow \infty} H(z_l(0), T_l) &= 0 \\ \Rightarrow \lim_{l \rightarrow \infty} \{z_l(0), T_l\} &= \{z_p(0), T_p\}. \end{aligned} \quad (\text{C19})$$

As the iteration step l increases, we find the periodic nonlinear solution.

We now compute $\{\Delta z_l(0), \Delta T_l\}$. We first examine the number of variables in $\{\Delta z_l(0), \Delta T_l\}$ versus the number of constraints in Eq.(C18). At first glance, there are $4N + 1$ variables but $4N$ constraints in Eq.(C18), which means that $\{\Delta z_l(0), \Delta T_l\}$ is indeterminate. However, we note that the solutions we seek are periodic in time. If $\{z_p(0), T_p\}$ is a periodic solution, so as $\{z_p(t \neq 0), T_p\}$ for an arbitrary initial time t . In other words, a phase condition has to be imposed to remove this arbitrariness. In our numerics, the phase condition is imposed by letting

$$\Delta z_l(0)|_{4N} = 0, \quad \forall l \geq 1, \quad (\text{C20})$$

and then in Eq.(C18) the numbers of variables and constraints match. Next, we elaborate the matrices appeared in Eq.(C18) as follows,

$$\frac{\partial H}{\partial T_l} = g(z_l(T_l)), \quad (\text{C21})$$

and

$$\frac{\partial H}{\partial z_l(0)} = \zeta(T_l) - I, \quad (\text{C22})$$

where $\zeta(t) \stackrel{\text{def}}{=} \partial z_l(t)/\partial z_l(0)$, and it is obvious that $\zeta(0) = I$. $\zeta(T_l)$ can be computed in the following way. We find that $d \ln \zeta/dt = M_l$, which in turn gives

$$\zeta(T_l) = \exp \int_0^{T_l} M_l(t) dt, \quad (\text{C23})$$

where the monodromy matrix M is defined as below

$$M = \partial g(z)/\partial z. \quad (\text{C24})$$

In our problem, each element of the monodromy matrix M is elucidated as follows,

$$\begin{aligned} M_{4n-3,4n-4} &= +dF_2(x)/dx|_{z_{4n-4}}, \\ M_{4n-3,4n-2} &= +\epsilon_0, \\ M_{4n-3,4n-0} &= +dF_1(x)/dx|_{z_{4n-0}}, \\ M_{4n-2,4n-5} &= -dF_2(x)/dx|_{z_{4n-5}}, \\ M_{4n-2,4n-3} &= -\epsilon_0, \\ M_{4n-2,4n-1} &= -dF_1(x)/dx|_{z_{4n-1}}, \\ M_{4n-1,4n-2} &= +dF_1(x)/dx|_{z_{4n-2}}, \\ M_{4n-1,4n-0} &= +\epsilon_0, \\ M_{4n-1,4n+2} &= +dF_2(x)/dx|_{z_{4n+2}}, \\ M_{4n-0,4n-3} &= -dF_1(x)/dx|_{z_{4n-3}}, \\ M_{4n-0,4n-1} &= -\epsilon_0, \\ M_{4n-0,4n+1} &= -dF_2(x)/dx|_{z_{4n+1}}. \end{aligned} \quad (\text{C25})$$

In summary, we employ Eqs.(C20, C21, C22), to solve $\{\Delta z_l(0), \Delta T_l\}$ in Eq.(C18) in every iteration step of shooting method.

So far, we have evolved a guessing solution into a periodic solution of certain small-amplitude A_1 . Our next

goal is to find nonlinear periodic solutions of the amplitudes greater than A_1 . Let us denote the above well-established nonlinear bulk mode as $\{z_p(0; A_1), T_p(A_1)\}$. We find nonlinear bulk modes of higher amplitudes by using the following strategy. We rescale the wave function by a uniform factor $1 + \xi$ ($\xi \ll 1$), to initialize shooting method with the new guessing solution,

$$\{z_1(0), T_1\} = \{(1 + \xi)z_p(0; A_1), T_p(A_1)\}. \quad (\text{C26})$$

Shooting method morphs it into a new periodic solution of the amplitude A_2 , which we denote $\{z_p(0; A_2), T_p(A_2)\}$. We note that A_2 is slightly greater than A_1 , but $A_2 \neq (1 + \xi)A_1$ because the trial wave function in Eq.(C26) is not a periodic solution. By repeating this strategy, we get nonlinear bulk modes for a wide range of amplitudes.

Having established the algorithm of shooting method, we now elaborate the numerical details of all parameters. Two sets of parameters of 1D generalized nonlinear Schrödinger equations are considered in this paper.

In the first set of parameters, the nonlinear model is subjected to reflection symmetry only. The on-site potential ϵ_0 adopted in Eqs.(A1) is $\epsilon_0 = 1.5$, and the parameters of nonlinear interactions in Eq.(C1) are specified as $c_1 = 0.25$, $c_2 = 0.37$, and $d_1 = 0.22$, $d_2 = 0.02$. We note that the topological attributes are not sensitive to the parameters. These parameters are randomly chosen. In order to numerically solve a nonlinear mode of wavenumber $q = 2\pi m/N$ ($m, N \in \mathcal{Z}$), we construct a chain of N unit cells composed of classical dimer fields, subjected to PBC. Consequently, the wavenumbers are rational numbers multiple of 2π . By constructing lattices with different unit cell numbers N , we initialize nonlinear modes with different wavenumbers. Since the wavenumbers $q = 2\pi \times (2m/2N) = 2\pi(m + N)/N = 2\pi m/N \bmod 2\pi$, we further restrict $0 \leq m \leq N - 1$, and $\text{gcd}(m, N) = 1$. We begin shooting method by employing the guessing perturbative solution $\{z_1(0), T_1\}$ in Eq.(C11), with the period T_1 , the wavenumber $q = 2\pi m/N$, and the small amplitude $A_1 \lesssim 10^{-1} \min(\sqrt{|c_1/d_1|}, \sqrt{|c_2/d_2|}, \sqrt{|(c_1 - c_2)/(d_1 - d_2)|})$. We simulate the differential equation by executing Runge-Kutta 6th-order[48] (RK6) and converting the time-differential operator $\partial/\partial t$ to the time-step $\Delta t = T_1/N_T$, where $N_T = 1000$. After N_T steps of the motion equations, the wave function should go back to the beginning state if it is a periodic solution. Thus, we compute the shooting function $H(z_1(0), T_1)$ to quantify how far away the wave function is from the periodic solution, and then slowly evolve the wave function towards it. $\eta_A = 300$ and $\eta_T = 10$ are adopted in Eq.(C16) to slow down the evolution process. In the l -th step of shooting method, the period is evolved to T_l , which in turn asks the time step to be $\Delta t = T_l/N_T$. In other words, we adjust the time difference Δt while keep the number of time steps N_T unchanged throughout the evolution procedure of shooting method. We keep evolving a nonlinear mode before the error of shooting

function e reaches the numerical tolerance e_{\max} ,

$$e \stackrel{\text{def}}{=} \frac{1}{4N} \sum_{i=1}^{4N} |H_i(z_l(0), T_l)| < e_{\max} = 3 \times 10^{-3}, \quad (\text{C27})$$

where H_i is the i th component of the $4N \times 1$ vector of shooting function, and e_{\max} is the numerical tolerance. In later discussions of this section, we will demonstrate the correspondence between the condition of $e < e_{\max}$ and the stability of nonlinear traveling waves by illustrating a stable mode ($e \ll e_{\max}$), a mode on the verge of stability ($e \lesssim e_{\max}$), and an unstable mode ($e > e_{\max}$) in fig.7. It is at this point that shooting method returns a periodic nonlinear traveling wave of amplitude A_1 and wavenumber $q = 2\pi m/N$. The next goal is to find periodic bulk modes of higher amplitudes. To this end, we uniformly rescale the aforementioned wave function by a factor of $1 + \xi$ ($\xi = 3 \times 10^{-3}$), to establish a new shooting procedure. Again, shooting method morphs the trial wave function into a traveling solution of amplitude A_2 . We repeat this strategy to obtain a series of nonlinear bulk modes with the given wavenumber $q = 2\pi m/N$ and a wide range of amplitudes.

Given the wave amplitude A , the nonlinear band structure $\omega = \omega(q \in [0, 2\pi], A)$ is plotted by selecting the eigenfrequencies of nonlinear bulk modes when the mode amplitudes A' are within the numerical tolerance,

$$|(A - A')/A| < \xi = 3 \times 10^{-3}. \quad (\text{C28})$$

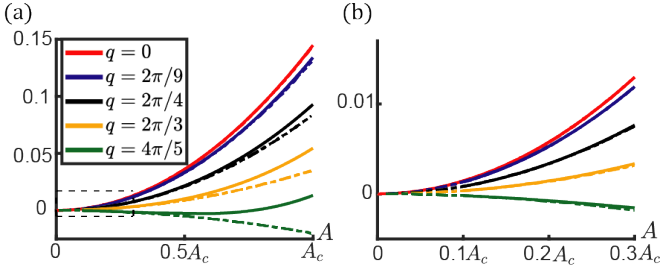


FIG. 6. Comparing shooting method (solid curves) and method of multiple-scale (dashed curves) on the frequency shift of nonlinear bulk waves. These nonlinear bulk modes start from $A = 0$ in the upper nonlinear band to A_c for a list of wavenumbers from $q = 0$ to $4\pi/5$. The model and interaction parameters are depicted by fig.1. Frequency shift computed by shooting method is $\delta\omega(q, A) = \omega(q, A) - \omega(q, A = 0)$, where $\omega(q, A)$ is the eigenfrequency of nonlinear bulk mode. Frequency shift obtained by method of multiple-scale is given by $\delta\omega(q, A) = D_1\theta$ in Eqs.(C10). (a) These two methods agree quite well in weakly nonlinear regime when $A \ll A_c$, while for $A \gtrsim 0.5A_c$, the large deviations demonstrate the breaking down of perturbation theory. (b) Enlarged data for $A \leq 0.3A_c$ encircled by the black dashed box in (a).

We now turn to discuss the stability analysis of nonlinear bulk modes. The stability analysis of nonlinear modes[36, 43] is to measure how many periods they persist in an undriven, undamped lattice before falling apart.

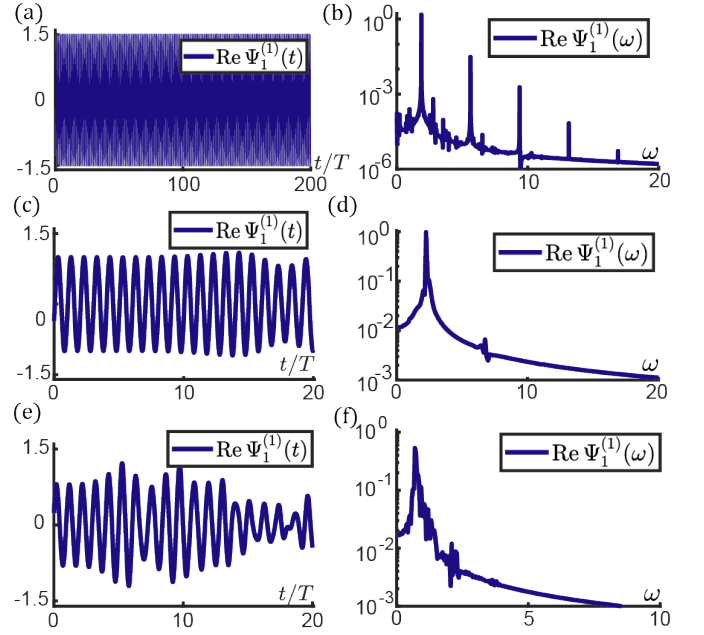


FIG. 7. Stability analysis of nonlinear bulk modes by performing the algorithm of self-oscillation. (a) A nonlinear bulk mode with the amplitude $A = 1.515$ and wavenumber $q = 4\pi/5$. The error of shooting function is $e = 10^{-6} \ll e_{\max} = 3 \times 10^{-3}$ (see Eq.(D1)), which suggests that the mode is stable. To verify our expectation, we initialize the mode from shooting method, and additionally impose a random perturbation $\delta\Psi_n^{(i)}$ on the wave function, where $\text{Re } \delta\Psi_n^{(i)}$ and $\text{Im } \delta\Psi_n^{(i)}$ are random numbers within 10^{-3} . The mode persists for more than 200 periods without generating other nonlinear modes, which demonstrates mode stability. We note that $A^2 \max(d_1, d_2) / \max(c_1, c_2) = 1.364$, which means the nonlinearities are larger than the linear parts of interactions. (b) The Fourier analysis of (a) after 200 periods provides additional evidence of mode stability. (c) A nonlinear bulk mode with $A = 0.9971$ and $q = 2\pi/9$. The error of shooting function is $e = 2.1 \times 10^{-3} < e_{\max}$, which suggests that the mode is on the verge of stability. We initialize the mode from shooting method without imposing any wave function perturbation. The mode persists for 15 periods (more than 13 periods[36]) before generating other modes and is therefore on the verge of stability. (d) The frequency spectrum of the mode in (c) manifests fundamental harmonic and frequency-tripling components. (e) A nonlinear bulk mode with $A = 0.8037$ and $q = 2\pi/21$. The error of shooting function is $e = 7.9 \times 10^{-3} > e_{\max}$, which indicates that the mode is unstable. The mode initialized by shooting method persists in 5 periods of oscillation, and it quickly exhibits mode instability by producing other nonlinear modes. (f) The frequency profile of (e) demonstrates the emergence of other Fourier components, which identifies mode instability.

According to Ref.[36], the mode is considered stable if an instability does not occur within 13 periods of oscillation. In order to perform the stability analysis for a nonlinear bulk mode with the wavenumber $q = 2\pi m/N$, we construct a lattice that comprises N dimer unit cells and is subjected to PBC. We establish a nonlinear bulk mode

obtained from shooting method. After letting the mode to oscillate by itself for more than 13 periods, Fourier analysis is applied to characterize whether the mode experiences instability and falls apart to other nonlinear modes. In fig.7, we exemplify three different bulk modes to verify the correspondence between Eq.(C27) and the mode stability. Hence, all nonlinear bulk modes depicted in the nonlinear band structures of figs.1(e, f) and fig.3(a) are considered stable, and they fulfill the criteria of the

nonlinear extension of adiabatic theorem[37–40].

In the second set of parameters, $c_1 = 0.25$, $c_2 = 0.37$, $d_1 = 0.22$, $d_2 = 0.02$ are carried over, while ϵ_0 is now set to zero. Nonlinear bulk modes always appear in $\pm\omega$ pairs. Similar to the linear counterpart in which charge-conjugation symmetry[5] is present, the eigenfrequencies of nonlinear topological boundary modes are zero in the second case.

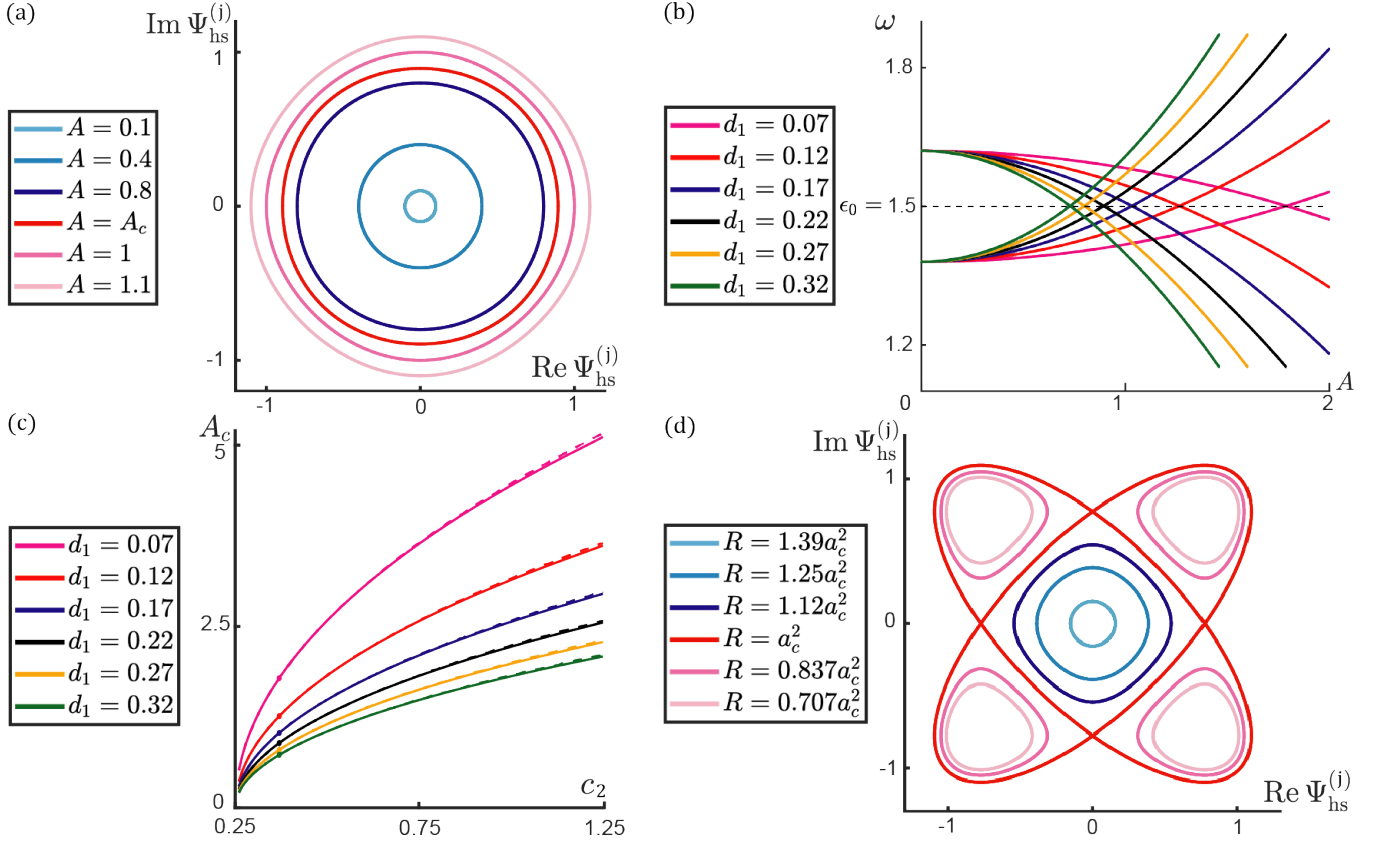


FIG. 8. (a) In the model with the parameters enumerated in fig.1, we plot the $(\text{Re } \Psi_{\text{hs}}^{(j)}, \text{Im } \Psi_{\text{hs}}^{(j)})$ trajectories for nonlinear bulk modes at high-symmetry points with a set of amplitudes ranging from $A = 0.1$ to 1.1 . The trajectories are noticeably different from regular circles for $A \gtrsim A_c$. (b) Transition amplitude A_c is numerically solved by Eq.(C34). Here, we exemplify these numerical solutions by varying d_1 from 0.07 to 0.32 , where the transition amplitude $A_c = 0.8944$ for $d_1 = 0.22$ is depicted by the intersection of black curves. All illustrated transition amplitudes occur at the merging frequency $\omega(\phi_\pi = 0, A_c) = \omega(\phi_\pi = \pi, A_c) = \epsilon_0$. (c) The nice agreement between numerically solved A_c (solid curves) and its estimation $A_c \approx \sqrt{4/3}a_c$ (dashed curves), where c_2 varies from 0.26 to 1.25 , and d_1 varies from 0.07 to 0.32 . The transition amplitudes in (b) are marked by colored dots here. We note that the estimations of A_c are worse for $c_2 \gtrsim 1.25$, which is much greater than $c_2 = 0.37$ in our model. (d) In the second case, all interaction parameters are the same as (a) except that $\epsilon_0 = 0$. We plot multiple $(\text{Re } \Psi_{\text{hs}}^{(j)}, \text{Im } \Psi_{\text{hs}}^{(j)})$ trajectories with the “constant of integration” R that varies from $1.39a_c^2$ to $0.707a_c^2$ (R is defined in Eq.(C30)). Blue and red curves describe nonlinear modes before and after instability occurs, respectively. The instability happens at $R = a_c^2$ which corresponds to mode amplitude $\max |\text{Re } \Psi_1^{(1)}| = a_c$. Above the instability point (i.e., $R < a_c^2$ and $\max |\text{Re } \Psi_1^{(1)}| > a_c$), wave functions oscillate around new equilibrium positions.

3. Topological transition amplitude A_c : calculating nonlinear bulk modes at high-symmetry points

In this subsection, we solve nonlinear bulk modes at high-symmetry points when $q_{\text{hs}} = 0, \pi$. This allows us to

numerically find the topological transition amplitude A_c as well as the band-touching frequency ω .

We denote the nonlinear bulk modes at high-symmetry points as Ψ_{hs} . According to Eq.(B8), the relative phase at high-symmetry points are $\phi_{\text{hs}} = 0$ or π . The motion equation of Ψ_{hs} is greatly simplified by employing Eqs.(B7, B14),

$$(i\omega\partial_\theta - \epsilon_0)\Psi_{\text{hs}}^{(j)} = e^{i\phi_{\text{hs}}} f_1(\Psi_{\text{hs}}^{(j')}, \Psi_{\text{hs}}^{(j)}) + e^{i(q_{\text{hs}} + \phi_{\text{hs}})} f_2(\Psi_{\text{hs}}^{(j')}, \Psi_{\text{hs}}^{(j)}), \quad (\text{C29})$$

for $j = 1, 2$. The nonlinear interactions are adopted from Eq.(C1). By solving Eq.(C29), $(\text{Re } \Psi_{\text{hs}}^{(j)}, \text{Im } \Psi_{\text{hs}}^{(j)})$ yield the trajectory,

$$[(\text{Re } \Psi_{\text{hs}}^{(j)})^2 - x_0]^2 + [(\text{Im } \Psi_{\text{hs}}^{(j)})^2 - x_0]^2 = R^2, \quad (\text{C30})$$

where R^2 is the constant of integration which quantifies the ‘‘radius’’ of the trajectory, and

$$x_0 = -\frac{\epsilon_0 + e^{i\phi_{\text{hs}}} c_1 + e^{i(q_{\text{hs}} + \phi_{\text{hs}})} c_2}{e^{i\phi_{\text{hs}}} d_1 + e^{i(q_{\text{hs}} + \phi_{\text{hs}})} d_2}. \quad (\text{C31})$$

In the small-amplitude limit, the trajectory simply reduces to a circle, which is in perfect agreement with linear models. Based on Eq.(C30), we further obtain the mode frequencies:

$$\omega(q_{\text{hs}}, \phi_{\text{hs}}) = \frac{\pi}{2} |d_1 + e^{iq_{\text{hs}}} d_2| \left[\int_0^A \frac{du}{y(u)\sqrt{|y(u) + e^{i\phi_{\text{hs}}} x_0|}} \right]^{-1}, \quad (\text{C32})$$

where A is the mode amplitude, and

$$y(u) = \sqrt{x_0^2 + (A^2 - x_0)^2 - (u^2 - x_0)^2}. \quad (\text{C33})$$

A quick check of the above result is to perform the integration in the weakly nonlinear regime when $A \ll \sqrt{|x_0|}$. Eq.(C32) reduces to $\omega = |\epsilon_0 + e^{i\phi_{\text{hs}}} c_1 + e^{i(q_{\text{hs}} + \phi_{\text{hs}})} c_2|$, which is in line with the high-symmetry eigenfrequencies in the linear models. In this paper, the numerical parameters we adopt yield $\epsilon_0, c_1, c_2, d_1, d_2 > 0$, and $c_1 < c_2, d_1 > d_2$. Thus, the topological phase transition occurs when the eigenfrequencies of nonlinear modes merge at the critical amplitude A_c when

$$\omega(\phi_\pi = 0, A_c) = \omega(\phi_\pi = \pi, A_c). \quad (\text{C34})$$

This transition amplitude A_c can be obtained by numerically solving the above equation, which is shown in fig.8(b).

Appendix D: Nonlinear topological boundary modes

In this section, we study nonlinear topological boundary modes based on the model of Eqs.(A1) with the interactions specified in Eq.(C1). To have topological boundary modes, we consider a semi-infinite lattice subjected to the open boundary condition (OBC)

$$\begin{aligned} i\partial_t \Psi_n^{(1)} &= \epsilon_0 \Psi_n^{(1)} + f_1(\Psi_n^{(1)}, \Psi_n^{(2)}) + f_2(\Psi_n^{(1)}, \Psi_{n-1}^{(2)}), \\ i\partial_t \Psi_n^{(2)} &= \epsilon_0 \Psi_n^{(2)} + f_1(\Psi_n^{(2)}, \Psi_n^{(1)}) + f_2(\Psi_n^{(2)}, \Psi_{n+1}^{(1)}), \\ \text{for } n \geq 1, \quad \text{and } \Psi_0^{(2)} &= 0. \end{aligned} \quad (\text{D1})$$

In subsections 1 and 2, we investigate topological edge modes for the model with $\epsilon_0 \neq 0$. In subsection 3, we explore topological modes for the vanishing on-site potential $\epsilon_0 = 0$. The parameters we consider yield $0 < c_1 < c_2, d_1 > d_2 > 0$.

1. Method of multiple-scale: topological edge modes for the $\epsilon_0 \neq 0$ case in weakly nonlinear regime

Based on the numerical simulation and qualitative analysis presented in the main text, it is demonstrated that the frequency of topological boundary mode is $\omega_{\text{T}} = \epsilon_0$ and is independent of the mode amplitude A . This result is in sharp contrast to the amplitude-dependent eigenfrequencies of nonlinear bulk modes. Here in weakly nonlinear regime, we quantitatively exhibit this result by employing the method of multiple-scale.

Method of multiple-scale introduces a book-keeping small parameter $\epsilon \ll 1$ that enforces small amplitudes for the boundary modes, which is practically realized by rewriting d_i as ϵd_i in the nonlinear interactions. The time derivative and the wave function are expanded in orders of ϵ (see Eqs.(C2, C3)). We expand the equations of motion and match them in orders of ϵ . The zeroth-order equations of motion are presented by Eq.(C4) respecting the OBC $\Psi_{0,(0)}^{(2)} = 0$. The zeroth-order solution reads

$$\Psi_{n,(0)} = -(-\kappa_0)^{n-1} A(T_{(1)}) e^{-i\omega_{\text{T}(0)} T_{(0)} - i\theta(T_{(1)})} (1, 0)^\top, \quad (\text{D2})$$

where $\kappa_0 = c_1/c_2$ and $\omega_{\text{T}(0)} = \epsilon_0$. The first-order equations of motion are given by Eq.(C7) subjected to the open boundary $\Psi_{0,(1)}^{(2)} = 0$. There are two parts in this first-order correction of the wave function, namely the fundamental harmonic part $\Psi_{n,(1)}(\omega_{\text{T}})$ and the frequency-tripling part $\Psi_{n,(1)}(3\omega_{\text{T}})$: $\Psi_{n,(1)} = \Psi_{n,(1)}(\omega_{\text{T}}) + \Psi_{n,(1)}(3\omega_{\text{T}})$. We are interested in the frequency correction due to the nonlinearities, which stems from the secular term generated by the fundamental harmonic part. The fundamental harmonics $\Psi_{n,(1)}(\omega_{\text{T}})$ obey the following recursive equations,

$$\begin{aligned} \Psi_{n,(1)}^{(2)}(\omega_{\text{T}}) + \frac{\Psi_{n-1,(1)}^{(2)}(\omega_{\text{T}})}{\kappa_0} + \frac{iD_1 A + AD_1 \theta}{(-\kappa_0)^{1-n} c_1} e^{-i\Phi} &= 0, \\ \Psi_{n,(1)}^{(1)}(\omega_{\text{T}}) + \frac{\Psi_{n+1,(1)}^{(1)}(\omega_{\text{T}})}{\kappa_0} - \frac{3(d_1 - d_2 \kappa_0^3) A^3 e^{-i\Phi}}{4(-\kappa_0)^{3-3n} c_1} &= 0, \end{aligned} \quad (\text{D3})$$

subjected to the OBC $\Psi_{0,(1)}^{(2)} = 0$, where the phase factor $\Phi = \omega_{\text{T}(0)} T_{(0)} + \theta(T_{(1)})$. If $D_1 A \neq 0$ or $D_1 \theta \neq 0$, Eqs.(D3) lead to the unphysical result that $\lim_{n \rightarrow \infty} |\Psi_{n,(1)}^{(2)}(\omega_{\text{T}})| \rightarrow \infty$. Hence Eqs.(D3) demand that $D_1 A = D_1 \theta = 0$. The result $D_1 \theta = 0$ demonstrates that the first-order correction of the eigenfrequency of the topological mode is zero. Up to the first-order correction, the frequency is

$$\omega_{\text{T}} = \omega_{\text{T}(0)} + \epsilon D_1 \theta = \epsilon_0, \quad (\text{D4})$$

which is independent of the mode amplitude. This conclusion is in line with the qualitative analysis and the numerical computation of nonlinear topological modes carried out in the main text. We note that $D_1 A = 0$ is the natural result of undamped systems. The total wave function up to the first-order correction is summarized as follows,

$$\begin{aligned}\Psi_n &= \Psi_{n,(0)} + \epsilon(\Psi_{n,(1)}, 0)^\top, \\ \Psi_{2n,(1)}^{(1)} &= \kappa_0^{2n-1} \frac{1 - \kappa_0^{4n-2}}{1 - \kappa_0^2} \frac{3(d_1 - d_2 \kappa_0^3) A^3 e^{-i\Phi}}{4c_1}, \\ \Psi_{2n+1,(1)}^{(1)} &= -\kappa_0^{2n} \frac{1 - \kappa_0^{4n}}{1 - \kappa_0^2} \frac{3(d_1 - d_2 \kappa_0^3) A^3 e^{-i\Phi}}{4c_1}.\end{aligned}\quad (\text{D5})$$

It is notable that the first-order correction of wave function exponentially decays in space and it does not diverge to infinity. In addition to this, the wave function in Eqs.(D5) fulfills Eq.(D9), which is the recursion relation of topological boundary modes in fully nonlinear regime. In summary, these results derived from the perturbative method of multiple-scale are in perfect agreement with the methods in fully nonlinear regime discussed in subsection 2.

2. Harmonic balance method: topological boundary modes for the $\epsilon_0 \neq 0$ case in fully nonlinear regime

We now employ the harmonic balance method[44] to study topological boundary modes in fully nonlinear regime. Since the mode is periodic in time, it can be expressed as the Fourier series $\Psi_n = \sum_l \psi_{l,n} e^{-i\omega_\tau t}$. We take the approximation by truncating the wave function to the fundamental harmonics,

$$\begin{aligned}\Psi_n &\approx \psi_{1,n} e^{-i\omega_\tau t} + \psi_{-1,n} e^{i\omega_\tau t} = \\ &\frac{1}{2} \begin{pmatrix} \alpha_n^{(1)} + i\alpha_n^{(2)} \\ \beta_n^{(1)} + i\beta_n^{(2)} \end{pmatrix} e^{-i\omega_\tau t} + \frac{1}{2} \begin{pmatrix} \alpha_n^{(1)*} + i\alpha_n^{(2)*} \\ \beta_n^{(1)*} + i\beta_n^{(2)*} \end{pmatrix} e^{i\omega_\tau t},\end{aligned}\quad (\text{D6})$$

where $\alpha_n = (\alpha_n^{(1)}, \alpha_n^{(2)})^\top$ and $\beta_n = (\beta_n^{(1)}, \beta_n^{(2)})^\top$ are 2×1 complex vectors parametrizing $\psi_{\pm 1,n}$. Hence, the real and imaginary parts of the wave functions can be expressed as

$$\begin{aligned}\text{Re } \Psi_n^{(1)} &= \frac{1}{2} \left(\alpha_n^{(1)} e^{-i\omega_\tau t} + \alpha_n^{(1)*} e^{i\omega_\tau t} \right), \\ \text{Im } \Psi_n^{(1)} &= \frac{1}{2} \left(\alpha_n^{(2)} e^{-i\omega_\tau t} + \alpha_n^{(2)*} e^{i\omega_\tau t} \right), \\ \text{Re } \Psi_n^{(2)} &= \frac{1}{2} \left(\beta_n^{(1)} e^{-i\omega_\tau t} + \beta_n^{(1)*} e^{i\omega_\tau t} \right), \\ \text{Im } \Psi_n^{(2)} &= \frac{1}{2} \left(\beta_n^{(2)} e^{-i\omega_\tau t} + \beta_n^{(2)*} e^{i\omega_\tau t} \right).\end{aligned}\quad (\text{D7})$$

We further truncate the equations of motion to the fundamental harmonics to find

$$\begin{aligned}(\epsilon_0 I + \omega_\tau \sigma_y) \alpha_n + \\ \begin{pmatrix} c_1(\sqrt{3}\beta_n^{(1)}/2)\beta_n^{(1)} + c_2(\sqrt{3}\beta_{n-1}^{(1)}/2)\beta_{n-1}^{(1)} \\ c_1(\sqrt{3}\beta_n^{(2)}/2)\beta_n^{(2)} + c_2(\sqrt{3}\beta_{n-1}^{(2)}/2)\beta_{n-1}^{(2)} \end{pmatrix} &= 0, \\ (\epsilon_0 I + \omega_\tau \sigma_y) \beta_n + \\ \begin{pmatrix} c_1(\sqrt{3}\alpha_n^{(1)}/2)\alpha_n^{(1)} + c_2(\sqrt{3}\alpha_{n+1}^{(1)}/2)\alpha_{n+1}^{(1)} \\ c_1(\sqrt{3}\alpha_n^{(2)}/2)\alpha_n^{(2)} + c_2(\sqrt{3}\alpha_{n+1}^{(2)}/2)\alpha_{n+1}^{(2)} \end{pmatrix} &= 0,\end{aligned}\quad (\text{D8})$$

where $\beta_0 = 0$, and $c_i(x) = c_i + d_i|x|^2$, $i = 1, 2$. We solve Eqs.(D8) by exploiting the approximation $\alpha_n \gg \beta_n$. By doing so, we obtain $\omega_\tau = \epsilon_0$, $\alpha_n^{(1)} = i\alpha_n^{(2)}$, $\arg \alpha_n^{(1)} = \arg \alpha_1^{(1)} + (n-1)\pi$, and

$$c_1(\sqrt{3}\alpha_n^{(j)}/2)\alpha_n^{(j)} + c_2(\sqrt{3}\alpha_{n+1}^{(j)}/2)\alpha_{n+1}^{(j)} = 0 \quad (\text{D9})$$

for $j = 1, 2$, which in turn demands that

$$c_1(\sqrt{3}\psi_{1,n}^{(1)}/2)|\psi_{1,n}^{(1)}| = c_2(\sqrt{3}\psi_{1,n+1}^{(1)}/2)|\psi_{1,n+1}^{(1)}|. \quad (\text{D10})$$

Consequently, the analytic waveform of nonlinear topological boundary mode is approximately solved as $\Psi_n \approx (\psi_{1,n}^{(1)}, 0)^\top e^{-i\epsilon_0 t}$. Let us denote $a_c = \sqrt{-(c_1 - c_2)/(d_1 - d_2)}$. If $|\psi_{1,1}^{(1)}| > \sqrt{4/3}a_c \approx A_c$, the mode keeps increasing and there is no topological boundary mode, whereas for $|\psi_{1,1}^{(1)}| < \sqrt{4/3}a_c \approx A_c$, a topological evanescent mode fades away from the boundary. On the other hand, Berry phase of nonlinear bulk modes changes at the critical amplitude A_c . Above this critical amplitude, Berry phase $\gamma(A > A_c) = 0$. Below the transition point, Berry phase $\gamma(A < A_c) = \pi$. The relationship between the emergence of topological boundary modes and Berry phase is the manifestation of the nonlinear extension of bulk-edge correspondence.

We now present the numerical details of exciting nonlinear topological boundary modes, given the parameters $\epsilon_0 = 1.5$, $c_1 = 0.25$, $c_2 = 0.37$, and $d_1 = 0.22$, $d_2 = 0.02$. We construct a lattice subjected to OBCs on both ends. The lattice consists of $N = 45$ unit cells to mimic a semi-infinite lattice. According to our theory, the lattice is in the topological phase when the bulk wave amplitude $A < A_c \approx \sqrt{4/3}a_c$. Bulk-edge correspondence demands that an evanescent mode should appear on lattice boundary, if the edge mode amplitude $\max(\text{Re } \Psi_1^{(1)}) < A_c$. Theoretical analysis indicates that the spatial profile of this edge mode shall obey Eq.(D10). We now attempt to numerically verify this result by exciting a topological boundary mode with amplitude $A < A_c$. To this end, a Gaussian tone burst

$$S_n = \delta_{n1} S e^{-i\omega_{\text{ext}} t - (t-t_0)^2/\tau^2} (1, 0)^\top \quad (\text{D11})$$

is applied on the open boundary at site $n = 1$, where the driving amplitude $S = 7 \times 10^{-2}$, the carrier frequency $\omega_{\text{ext}} = \epsilon_0$, the mode period $T = 2\pi/\omega_{\text{ext}}$, the half height width $\tau = 3T$, and $t_0 = 15T$. In order to confirm the

steadystate conditions, we wait $5000T$ before making any wave function measurements. We compute the frequency spectrum $\text{Re } \Psi_1^{(1)}(\omega)$ by performing fast Fourier transformation (FFT) for the time interval $t \in [10, 5000]T$ in fig.2(d). In fig.2(e), we plot the spatial profile of the amplitude of the boundary excitation, $\max(\text{Re } \Psi_n^{(1,2)}(t))$. In

fig.2(f), we plot the spatial profile of the Fourier component $\text{Re } \Psi_n^{(1,2)}(\omega = \epsilon_0)$. The curves are in perfect agreement with the theoretical predictions of nonlinear topological mode $\Psi_n \approx (\psi_{1,n}^{(1)}, 0)^\top e^{-i\epsilon_0 t}$, where $\psi_{1,n}^{(1)}$ are computed by Eq.(D10).

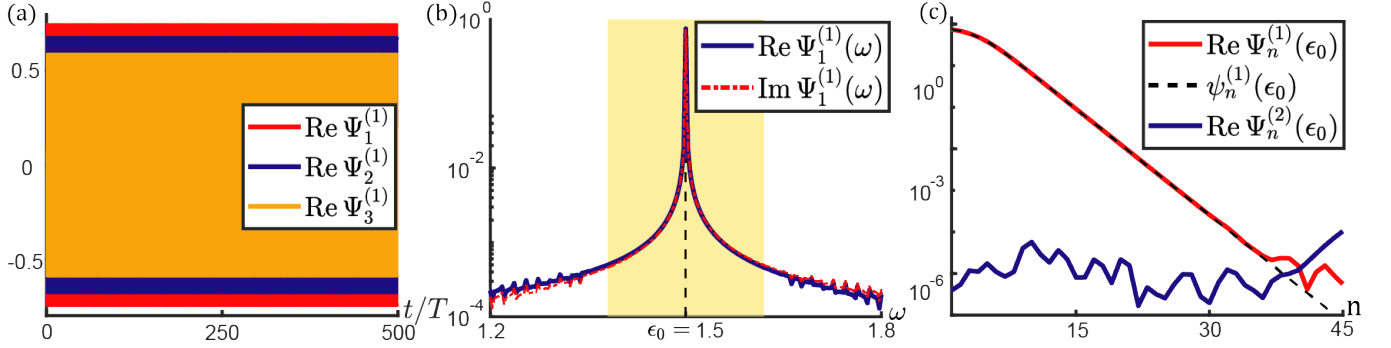


FIG. 9. Stability analysis of nonlinear topological evanescent modes by performing the algorithm of self-oscillation in an undamped, undriven lattice. The lattice is constructed from $N = 45$ unit cells subjected to OBC on both ends to mimic a semi-infinite lattice. The parameters of interactions are carried over from fig.1 of the main text, namely $\epsilon_0 = 1.5$, $c_1 = 0.25$, $c_2 = 0.37$, $d_1 = 0.22$, and $d_2 = 0.02$. (a) A nonlinear topological boundary mode with amplitude $\text{Re } \Psi_1^{(1)} = 0.75 < A_c$. The mode is initialized by its analytic approximating form $\Psi_n \approx (\psi_{1,n}^{(1)}, 0)^\top e^{-i\epsilon_0 t}$ derived from Eq.(D10), and is truncated in the finite lattice. The mode is allowed to self-oscillate in the lattice for more than $500T$, where $T = 2\pi/\epsilon_0$ is the theoretical prediction of the period. (b) Fourier analysis of the topological mode in frequency space, where the peak is in perfect agreement with $\omega_T = \epsilon_0$, our theoretical anticipation of the mode frequency. The yellow shaded area is the linear band structure $|\epsilon_0 + c_1 - c_2| < \omega < |\epsilon_0 - c_1 + c_2|$. (c) Red and blue curves stand for the spatial profile of the peaks at $\omega = \epsilon_0$ of the Fourier components of the unit cells. Black dashed line is the analytic approximating solution $\Psi_n \approx (\psi_{1,n}^{(1)}, 0)^\top e^{-i\epsilon_0 t}$ derived from Eq.(D10).

The stability analysis of nonlinear topological boundary modes is similar to what has been done in nonlinear bulk modes. We construct a lattice that is composed of $N = 45$ unit cells and is subjected to the OBCs on both ends, to mimic a semi-infinite lattice. We initialize the topological mode by employing the analytic approximating solution $\Psi_n \approx (\psi_{1,n}^{(1)}, 0)^\top e^{-i\epsilon_0 t}$ derived from Eq.(D10). After more than 13 periods of self-oscillation in the undamped, undriven lattice, we perform Fourier analysis to characterize if the mode has fallen apart to other nonlinear modes. As shown in fig.9, the mode remains intact for more than $500T$, which demonstrates mode stability. What is more, all features of this nonlinear topological mode, including the eigenfrequency and the spatial profile of mode amplitude, are in perfect alignment with the approximated theoretical solution of Eq.(D10).

According to our theory, nonlinear topological modes do not exist if $\max(\text{Re } \Psi_1^{(1)}) > A_c$. We numerically verify this by driving the lattice boundary with a Gaussian

tone burst (Eq.(D11)), where the stimulation amplitude is $S = 53 \times 10^{-2}$. As shown in figs.2(g), (h), the amplitude of the responding signal is nearly the same for sites $n = 1, 10$, and 20 , and the frequency spectrum comprises bulk modes. We note that due to the large amplitude of excitation, the responding nonlinear mode quickly shows instability[27] and falls apart to other nonlinear modes. To have a stable responding signal, we introduce small damping $\eta = 10^{-3}$ for this large-amplitude driven case. Damping is ubiquitous in dissipative classical systems (see Eqs.(E11) and Eqs.(??) for example).

Fig.10 studies nonlinear topological boundary modes in disordered lattice where the bond connecting $\Psi_7^{(1)}$ and $\Psi_7^{(2)}$ is replaced by the interaction $f'_1(\Psi_7^{(1)}, \Psi_7^{(2)}) = c'_1 \Psi_7^{(2)} + d'_1 [(\text{Re } \Psi_7^{(2)})^3 + i(\text{Im } \Psi_7^{(2)})^3]$. The topologically protected boundary mode is insensitive to disorder, in the sense that there is no change of frequency (i.e., $\omega_T = \epsilon_0$), and the excitation is still robust.

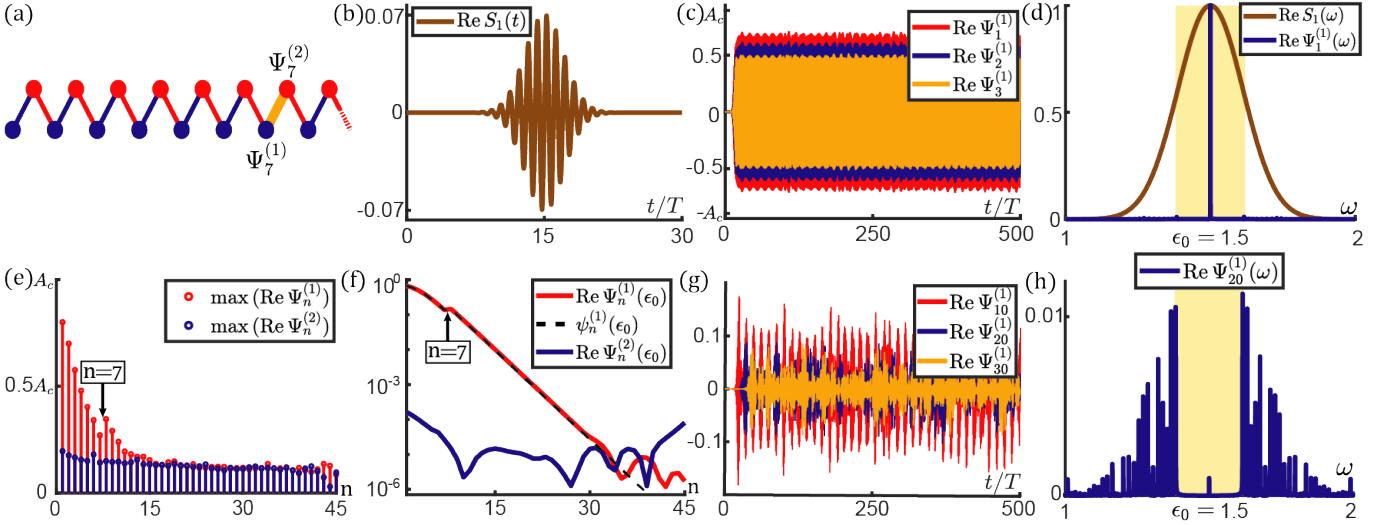


FIG. 10. Exciting topological edge modes in disordered nonlinear SSH lattice. The interaction parameters $\epsilon_0, c_1, c_2, d_1$ and d_2 are the same as fig.1. (a) We construct a long chain that consists of $N = 45$ unit cells and is subjected to the OBCs on both ends to mimic a semi-infinite lattice. Red and blue bonds stand for nonlinear interactions between nearest neighbors. The disorder is introduced by replacing the blue bond with an orange one connecting $\Psi_7^{(1)}$ and $\Psi_7^{(2)}$, where the interaction parameters are replaced by $c_1' = 0.4$ and $d_1' = 0.15$. (b) A Gaussian tone burst is employed on the first site to excite topological boundary mode, where all parameters of this driving signal are carried over from fig.2(b). (c) Wave functions of $n = 1, 2, 3$ sites exhibit the localization of topological mode, where the amplitude $\max(\text{Re } \Psi_1^{(1)}) < A_c$. (d) Brown and blue curves represent the frequency profiles of Gaussian shaking and responding mode of site $n = 1$, respectively. Yellow shaded area is the linear bandgap. Despite the disorder, the frequency of topological mode is still $\omega_T = \epsilon_0 = 1.5$. (e) The spatial profile of mode amplitude captures a noticeable jump at site $n = 7$ which stems from the disorder. (f) Red and blue curves are the spatial profiles of the $\omega = \epsilon_0$ wave component, where the noticeable jump is presented in the $\text{Re } \Psi_n^{(1)}(\epsilon_0)$ curve at the 7th site. The analytic prediction of the topological mode $\psi_n^{(1)}(\epsilon_0)$ is described by the black dashed line, which is in perfect agreement with numerical results. (g) The wave functions of $n = 10, 20, 30$ sites exhibit echolike shapes indicating multiple reflections at the boundaries, which in turn show the bulk mode excitations. These bulk mode components are excited by the input Gaussian tone burst in (b) which contains all frequencies. (h) The frequency spectrum indicates that the mode at site $n = 20$ is mainly composed of bulk modes.

3. Exact solution of static nonlinear topological boundary modes for the $\epsilon_0 = 0$ case

In contrast to the $\epsilon_0 \neq 0$ model, this $\epsilon_0 = 0$ model features two qualitatively different properties.

The first property lies in the lattice under PBC. At the critical amplitude a_c , the nonlinear bands merge at zero-frequency. When the mode amplitude goes beyond this critical amplitude, the lattice experiences instability to reach new ground states. There are eight new ground states described by the equilibrium wave functions,

$$\bar{\Psi}_n = (-1)^n \sqrt{2} a_c (e^{is_1 \pi/4}, s_2 e^{is_3 \pi/4})^\top, \quad (\text{D12})$$

where $s_1, s_2, s_3 = \pm 1$. Without loss of generality, we pick one of the eight equilibrium ground states, $\bar{\Psi}_n = (-1)^n e^{i\pi/4} \sqrt{2} a_c (1, 1)^\top$, to study small fluctuations $\delta\Psi_n = \Psi_n - \bar{\Psi}_n$ around it. By expanding the equations to the linear order in $\delta\Psi_n$, we obtain

$$H_q \delta\Psi_q = i\partial_t \delta\Psi_q, \quad (\text{D13})$$

where $\delta\Psi_q = \sum_n \delta\Psi_n e^{-iqn}$ is the momentum-space wave function, and the new ground state Hamiltonian H_q reads

$$H_q = [c_1(\sqrt{3}a_c) + c_2(\sqrt{3}a_c) \cos q] \sigma_x + [c_2(\sqrt{3}a_c) \sin q] \sigma_y. \quad (\text{D14})$$

The second peculiar property is that the nonlinear topological boundary modes are static in time, which allows for analytic solutions governed by the following nonlinear recursion relations,

$$\begin{aligned} c_1(\text{Re } \Psi_n^{(1)})|\text{Re } \Psi_n^{(1)}| &= c_2(\text{Re } \Psi_{n+1}^{(1)})|\text{Re } \Psi_{n+1}^{(1)}|, \\ c_1(\text{Im } \Psi_n^{(1)})|\text{Im } \Psi_n^{(1)}| &= c_2(\text{Im } \Psi_{n+1}^{(1)})|\text{Im } \Psi_{n+1}^{(1)}|, \\ c_1(\text{Re } \Psi_n^{(2)})|\text{Re } \Psi_n^{(2)}| &= c_2(\text{Re } \Psi_{n-1}^{(2)})|\text{Re } \Psi_{n-1}^{(2)}|, \\ c_1(\text{Im } \Psi_n^{(2)})|\text{Im } \Psi_n^{(2)}| &= c_2(\text{Im } \Psi_{n-1}^{(2)})|\text{Im } \Psi_{n-1}^{(2)}|, \end{aligned} \quad (\text{D15})$$

subjected to the OBC $\Psi_0^{(2)} = 0$.

Stability analysis of topological modes is elaborated as follows. We construct a lattice with $N = 45$ unit

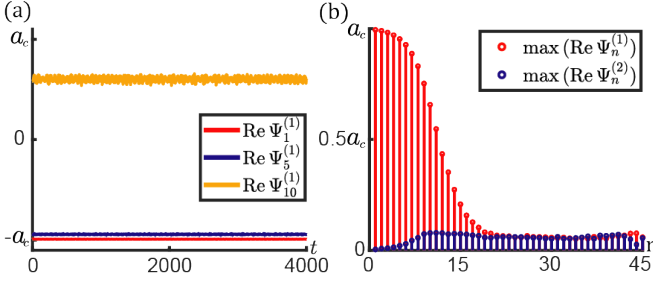


FIG. 11. Stability analysis of nonlinear topological boundary modes. (a) Temporal profile of the perturbed topological mode for the time interval $t \in [0, 75 \times 2\pi/(c_2 - c_1)]$. The mode remains intact without generating other wave components, which demonstrates mode stability. (b) Spatial profile of the amplitude of the mode on each site.

cells subjected to the OBCs on both ends, and initialize the mode via the following procedure. We establish the analytic solution of Eqs.(D15) with the amplitude $\text{Re } \Psi_1^{(1)} = \text{Im } \Psi_1^{(1)} = 0.99a_c$. Next, we perturb the aforementioned mode by multiplying a random factor $1 + \xi_n$ ($\xi_n \leq 10^{-2}$) on the wave function of each site n . Finally, we let the initialized mode to self-oscillate in the undamped, undriven lattice. We wait $t = 75 \times 2\pi/(c_2 - c_1)$ before making any wave function measurements. As shown in fig.11, the mode remains intact without producing other wave components, which demonstrates the stability of nonlinear topological boundary modes.

Appendix E: Deriving generalized nonlinear Schrödinger equations for three classical models

In this section, we derive the nonlinear equations of motion for two classical structures that exhibit topological properties.

1. Topological photonics

The first model is proposed in Refs.[45, 46]. As shown in fig.4, the model is a 1D array of waveguides to propagate electric waves along the axial z -direction without backscattering. The unit cell comprises two waveguides coupled between nearest neighbors, and the coupling is the nonlinear function of complex amplitudes of electric fields. By denoting the wave amplitudes as $\Psi_n^{(1)}$ and $\Psi_n^{(2)}$, the equations of motion are governed by generalized nonlinear Schrödinger equations

$$\begin{aligned} i\partial_z \Psi_n^{(1)} &= \epsilon_0 \Psi_n^{(1)} + \kappa_1(\Psi_n^{(1)}, \Psi_n^{(2)}) + \kappa_2(\Psi_n^{(1)}, \Psi_{n-1}^{(2)}), \\ i\partial_z \Psi_n^{(2)} &= \epsilon_0 \Psi_n^{(2)} + \kappa_1(\Psi_n^{(2)}, \Psi_n^{(1)}) + \kappa_2(\Psi_n^{(2)}, \Psi_{n+1}^{(1)}), \end{aligned} \quad (\text{E1})$$

where κ_1 and κ_2 are intra and inter cell couplings and are nonlinear functions of the wave amplitudes. The model

is subjected to reflection symmetry, in the meaning that the equations of motion are invariant under the change of field variables $(\Psi_n^{(1)}, \Psi_n^{(2)}) \rightarrow (\Psi_{-n}^{(2)}, \Psi_{-n}^{(1)})$. Thus, Berry phase of nonlinear bulk modes is quantized and the nonlinear topological modes manifest themselves on the open boundaries of this 1D array. We now write $\kappa_i(x, y)$ as the summation of two polynomials,

$$\kappa_i(x, y) = g_i(x, y)x + h_i(y). \quad (\text{E2})$$

Hence, $g_i(x, y)$ effectively makes a correction to the on-site potential ϵ_0 . We further take the large- ϵ_0 limit by assuming that $g_i(x, y)/\epsilon_0 \ll 1$. Eqs.(E1) are simplified as

$$\begin{aligned} i\partial_z \Psi_n^{(1)} &= \epsilon_0 \Psi_n^{(1)} + h_1(\Psi_n^{(2)}) + h_2(\Psi_{n-1}^{(2)}), \\ i\partial_z \Psi_n^{(2)} &= \epsilon_0 \Psi_n^{(2)} + h_1(\Psi_n^{(1)}) + h_2(\Psi_{n+1}^{(1)}), \end{aligned} \quad (\text{E3})$$

to realize the minimal model of nonlinear topological chain presented in this paper.

2. Topoelectrical circuit

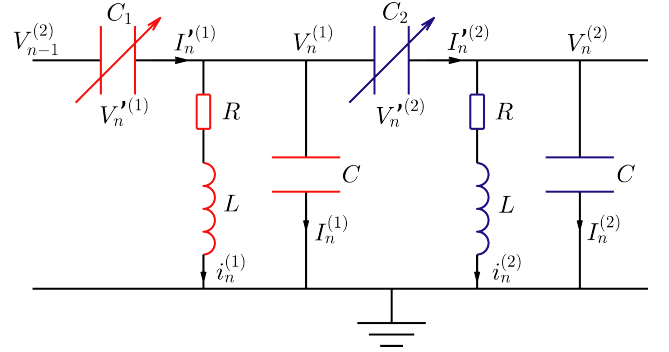


FIG. 12. The unit cell of nonlinear topoelectrical circuit. It is composed of two pairs of LC resonators of natural frequency ω_0 , which are connected by nonlinear capacitors $C_j = C_j(V)$ for $j = 1, 2$.

Here, we demonstrate that the equations of motion of 1D nonlinear topoelectrical circuit can be converted to generalized nonlinear Schrödinger equations. As we show in fig.12, the unit cell of the ladder circuit is composed of two resonators of natural frequency $\omega_0 = 1/\sqrt{LC}$, where L is the inductance and C is the capacitance. The resonators are connected by nonlinear capacitors $C_j = C_j(V)$ for $j = 1, 2$ as the functions of their voltages. We denote the voltages of the resonators as $V_n^{(j)}$, the currents of the inductances as $i_n^{(j)}$, and the currents of the capacitors as $I_n^{(j)}$. We further denote the voltages and currents of the nonlinear capacitors as $V_n'^{(j)}$ and $I_n'^{(j)}$,

respectively. Kirchhoff's law tells us

$$\begin{aligned} V_n^{(1)} &= V_{n-1}^{(2)} - V_n^{(1)}, \\ V_n^{(2)} &= V_n^{(1)} - V_n^{(2)}, \\ I_n^{(1)} &= i_n^{(1)} + I_n^{(1)} + I_n^{(2)}, \\ I_n^{(2)} &= i_n^{(2)} + I_n^{(2)} + I_{n+1}^{(1)}. \end{aligned} \quad (\text{E4})$$

We also have

$$\begin{aligned} I_n^{(j)} &= C \dot{V}_n^{(j)}, \\ I_n^{(j)} &= C_{j,n} \dot{V}_n^{(j)}, \end{aligned} \quad (\text{E5})$$

for $j = 1, 2$, where $C_{j,n} = C_j(V_n^{(j)})$ are the nonlinear capacitances. By adopting the limit of small nonlinear capacitances[8] $C_{j,n} \ll C$, from Eqs.(E4, E5) we obtain

$$\begin{aligned} i_n^{(1)} &\approx C_{1,n} \dot{V}_{n-1}^{(2)} + C_{2,n} \dot{V}_n^{(2)} - C \dot{V}_n^{(1)}, \\ i_n^{(2)} &\approx C_{1,n+1} \dot{V}_{n+1}^{(1)} + C_{2,n} \dot{V}_n^{(1)} - C \dot{V}_n^{(2)}. \end{aligned} \quad (\text{E6})$$

The equations of motion for the inductances are

$$L \dot{i}_n^{(j)} + R i_n^{(j)} = V_n^{(j)}. \quad (\text{E7})$$

Finally, we employ the approximation $C_{j,n} \ll C$ again to

Appendix F: An analytically solvable topological model with Kerr-type nonlinear interactions

We study an alternative model to provide additional verification of the nonlinear topological theory presented in this paper. The model is analytically solvable, in the sense that the nonlinear bulk modes as well as the dispersion relation can be exactly solved. The model is based on Eqs.(A1) with the Kerr-type nonlinearities[49]

$$f_i(x, y) = c_i y + d_i |y|^2 y, \quad i = 1, 2, \quad (\text{F1})$$

where the parameters yield $0 < c_1 < c_2$ and $d_1 > d_2 > 0$. This model is subjected to reflection symmetry. According to the main text, reflection symmetry demands the quantization of Berry phase of nonlinear bulk modes, regardless of the functional forms of interactions. This conclusion should remain valid for Kerr-type nonlinearities. To verify the quantization of Berry phase, we solve nonlinear traveling modes as below,

$$\Psi_n = A(1, e^{-i\phi_q})^\top e^{iqn - i\omega t}, \quad (\text{F2})$$

simplify Eqs.(E1) as follows,

$$\begin{aligned} \frac{\ddot{V}_n^{(1)}}{\omega_0^2} + RC \dot{V}_n^{(1)} &= -V_n^{(1)} - \frac{C_{1,n}}{C} V_{n-1}^{(2)} - \frac{C_{2,n}}{C} V_n^{(2)}, \\ \frac{\ddot{V}_n^{(2)}}{\omega_0^2} + RC \dot{V}_n^{(2)} &= -V_n^{(2)} - \frac{C_{1,n+1}}{C} V_{n+1}^{(1)} - \frac{C_{2,n}}{C} V_n^{(1)}. \end{aligned} \quad (\text{E8})$$

We then express the voltages as the envelope function

$$V_n^{(j)} = \Psi_n^{(j)} e^{-i\omega_0 t} \quad (\text{E9})$$

which in turn gives us

$$\begin{aligned} \ddot{\Psi}_n^{(j)} &= (\ddot{\Psi}_n^{(j)} - 2i\omega_0 \dot{\Psi}_n^{(j)} - \omega_0^2 \Psi_n^{(j)}) e^{-i\omega_0 t} \\ &\approx (-2i\omega_0 \dot{\Psi}_n^{(j)} - \omega_0^2 \Psi_n^{(j)}) e^{-i\omega_0 t}, \end{aligned} \quad (\text{E10})$$

where in the second step we assume that the time-modulation of $V_n^{(j)}$ is mostly captured by the factor $e^{-i\omega_0 t}$ and hence $\Psi_n^{(j)}$ varies slowly in time, giving $\ddot{\Psi}_n^{(j)} \ll \omega_0 \dot{\Psi}_n^{(j)}$. We denote the damping coefficient $\eta = RC\omega_0/2 \ll 1$ for simplicity. It is at this point that we obtain the equations of motion which is expressed as generalized nonlinear Schrödinger equations with small damping

$$\begin{aligned} (i - \eta) \dot{\Psi}_n^{(1)} + i\eta\omega_0 \Psi_n^{(1)} &= \frac{\omega_0 C_{1,n}}{2C} \Psi_{n-1}^{(2)} + \frac{\omega_0 C_{2,n}}{2C} \Psi_n^{(2)}, \\ (i - \eta) \dot{\Psi}_n^{(2)} + i\eta\omega_0 \Psi_n^{(2)} &= \frac{\omega_0 C_{1,n+1}}{2C} \Psi_{n+1}^{(1)} + \frac{\omega_0 C_{2,n}}{2C} \Psi_n^{(1)}, \end{aligned} \quad (\text{E11})$$

where the coupling terms serve as nonlinear interactions of field variables $\Psi_n^{(j)}$.

where the dispersion relation is

$$\omega = \epsilon_0 \pm \sqrt{c_1(A)^2 + c_2(A)^2 + 2c_1(A)c_2(A) \cos q}, \quad (\text{F3})$$

$c_i(A) = c_i + d_i A^2$, and the relative phase ϕ_q is

$$\phi_q = \arctan \left(\frac{-c_2(A) \sin q}{c_1(A) + c_2(A) \cos q} \right). \quad (\text{F4})$$

Following the convention of Fourier transformation in Eq.(A8), the Fourier components of the sinusoidal nonlinear bulk mode are $\psi_{l,q}^{(1)} = \psi_{l,q}^{(2)} = A\delta_{l,1}$. According to Eq.(F3), the nonlinear bandgap never closes unless the wave amplitude hits the topological transition point a_c . Apart from a_c , Berry phase of nonlinear bulk modes is well-defined, and can be greatly simplified to the following result by employing the sinusoidal form of nonlinear waves,

$$\gamma(A) = \frac{1}{2} i \oint_{\text{BZ}} dq \partial_q \ln [c_1(A) + c_2(A) e^{iq}]. \quad (\text{F5})$$

According to our general theory, Berry phase is expected to be $\gamma(A < a_c) = \pi$ and $\gamma(A > a_c) = 0$, which

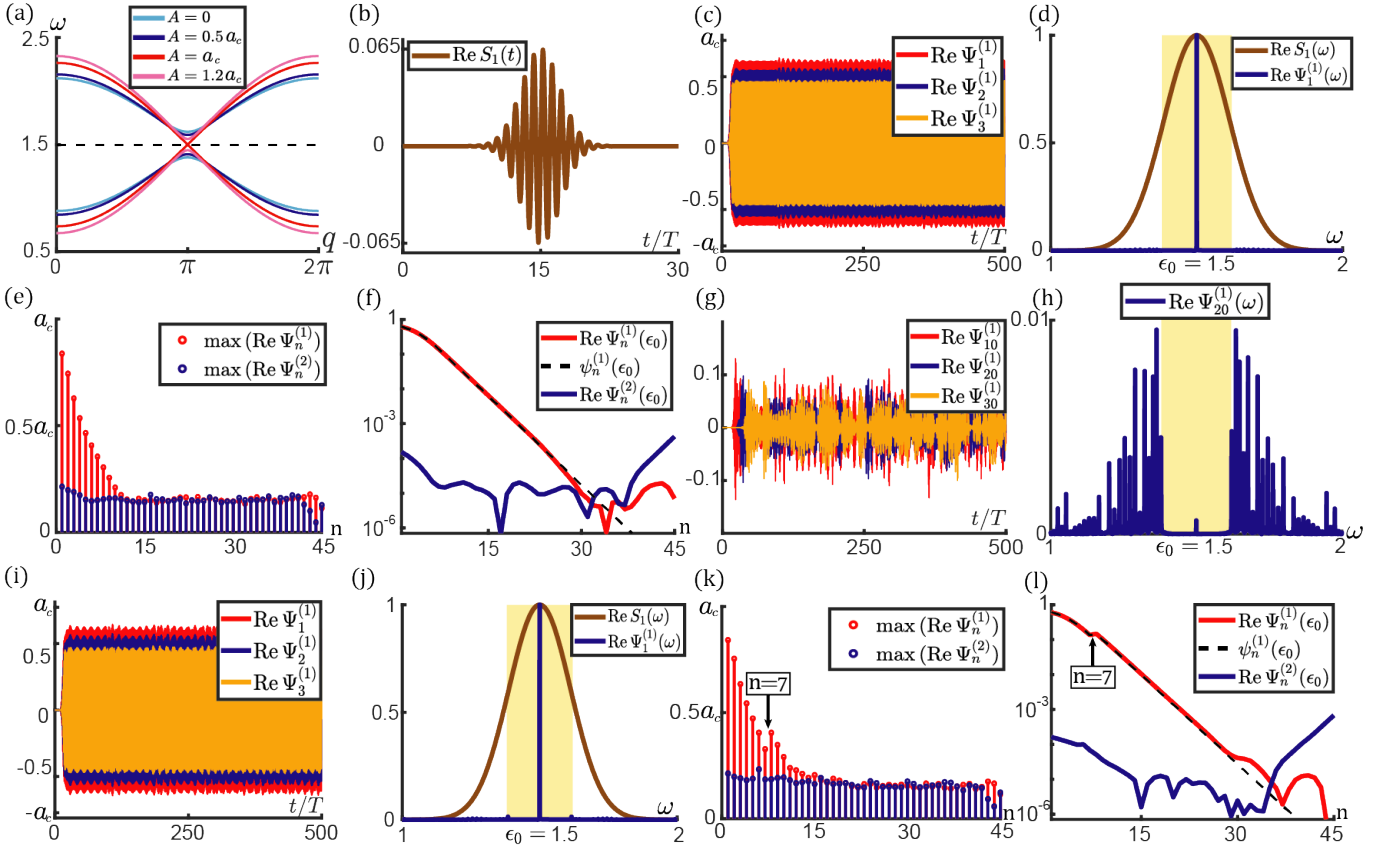


FIG. 13. Topological properties of nonlinear SSH lattice subjected to Kerr-type nonlinearities. The interaction parameters, including ϵ_0 , c_1 , c_2 , d_1 and d_2 , are the same as those in fig.1. (a) Nonlinear band structures for various amplitudes ranging from $A = 0$ to $1.2a_c$, where $a_c = \sqrt{-(c_2 - c_1)/(d_2 - d_1)} = 0.7746$. The nonlinear bands touch at the critical amplitude $A = a_c$, and Berry phase changes abruptly from $\gamma(A < a_c) = \pi$ to $\gamma(A > a_c) = 0$. (b) By constructing a finite lattice shown in fig.2(a) with open boundary conditions, we shake the boundary on site $n = 1$ by imposing a Gaussian tone burst in Eq.(D11) to excite nonlinear topological modes, where $S = 6.5 \times 10^{-2}$, $\omega_{\text{ext}} = \epsilon_0 = 1.5$, $T = 2\pi/\omega_{\text{ext}}$, $\tau = 3T$, and $t_0 = 15T$. (c) Responding mode on $n = 1, 2, 3$ sites indicates the mode localization, where the mode amplitude $\max(\text{Re } \Psi_n^{(1)}) < a_c$. (d) Brown and blue curves stand for the frequency spectra of external Gaussian signal and $n = 1$ site responding wave function. Yellow shaded area is the linear bandgap. (e) Spatial profile of the boundary excitation amplitude. We note that the bulk mode components reflected here are excited by Gaussian signal, which contains all frequencies. (f) Red and blue curves are the spatial profiles of the $\omega = \epsilon_0$ Fourier component of the boundary mode, The analytic result of the $\omega = \epsilon_0$ Fourier component is depicted by the black dashed curve. (g) The echolike wave functions of sites $n = 10, 20, 30$ manifest bulk mode components excited by the external Gaussian shaking signal. (h) The spectrum of $n = 20$ site contains a wide range of frequency components of bulk modes. (i) We now study topological edge modes in the disordered lattice depicted by fig.10(a), where the interaction parameters c'_1 and d'_1 of the disordered bond at site $n = 7$ are carried over from that figure. Responding modes are plotted for $n = 1, 2, 3$ sites which exhibit the feature of mode localization. (j) Fourier analysis of frequency space for wave function at site $n = 1$. (k) Spatial profile of the responding amplitudes. A noticeable bump at site $n = 7$ is induced by the disorder. (l) Spatial profile of the $\omega = \epsilon_0$ frequency component is captured by red and blue curves, and the theoretical analysis of this component is described by the black dashed curve.

holds true for arbitrary reflection-symmetric 1D systems and is independent of the functional forms of nonlinearities. This result is verified by evaluating Eq.(F5) for Kerr-type nonlinear interactions.

As stated by the nonlinear extension of bulk-edge correspondence, nonlinear topological modes should emerge on the lattice open boundary when the bulk band is topologically non-trivial with Berry phase $\gamma = \pi$, whereas topological modes disappear when $\gamma = 0$. Here we con-

firm this correspondence by studying the attributes of nonlinear topological boundary modes. To this end, we Fourier transform the edge mode into frequency space, and truncating it to the fundamental harmonics,

$$\Psi_n \approx \psi_{-1,n} e^{i\omega t} + \psi_{1,n} e^{-i\omega t}. \quad (\text{F6})$$

Similarly, the nonlinear terms in the interactions are

truncated as follows,

$$|\Psi_n^{(j)}|^2 \Psi_n^{(j)} \approx (|\psi_{-1,n}^{(j)}|^2 + 2|\psi_{1,n}^{(j)}|^2) \psi_{-1,n}^{(j)} e^{i\omega t} + (2|\psi_{-1,n}^{(j)}|^2 + |\psi_{1,n}^{(j)}|^2) \psi_{1,n}^{(j)} e^{-i\omega t}. \quad (\text{F7})$$

Consequently, the equations of motion reduce to the following nonlinear recursion relations,

$$\begin{aligned} (\epsilon_0 - s\omega) \psi_{s,n}^{(1)} + C_1(\psi_{s,n}^{(2)}) + C_2(\psi_{s,n-1}^{(2)}) &= 0, \\ (\epsilon_0 - s\omega) \psi_{s,n}^{(2)} + C_1(\psi_{s,n}^{(1)}) + C_2(\psi_{s,n+1}^{(1)}) &= 0, \end{aligned} \quad (\text{F8})$$

where $s = \pm 1$, and

$$C_i(\psi_{s,n}^{(j)}) = c_i \psi_{s,n}^{(j)} + d_i (|\psi_{s,n}^{(j)}|^2 + 2|\psi_{-s,n}^{(j)}|^2) \psi_{s,n}^{(j)}. \quad (\text{F9})$$

We exploit the approximation $\psi_{s,n}^{(1)} \gg \psi_{s,n}^{(2)}$, which is numerically verified in fig.13(f). We solve Eqs.(F8) to find

$\omega = \epsilon_0$, $\psi_{-1,n}^{(1)} = 0$ for all n , $\text{Arg} \psi_{1,n}^{(1)} = \text{Arg} \psi_{1,1}^{(1)} + (n-1)\pi$, and

$$c_1(\psi_{1,n}^{(1)}) |\psi_{1,n}^{(1)}| = c_2(\psi_{1,n+1}^{(1)}) |\psi_{1,n+1}^{(1)}|, \quad (\text{F10})$$

where $c_i(x) = c_i + d_i |x|^2$. Based on Eq.(F10), when $|\psi_{1,1}^{(1)}| < a_c$, an evanescent mode fades away from the lattice boundary, whereas for $|\psi_{1,1}^{(1)}| > a_c$, an unphysical mode quickly diverges to infinity and therefore cannot exist. The emergence and disappearance of boundary modes are in accordance with topologically non-trivial and trivial Berry phases, which is the manifestation of bulk-edge correspondence with Kerr-type nonlinearities.

-
- [1] F. D. M. Haldane, Phys. Rev. Lett. **61**, 2015 (1988).
[2] L. Fu, C. L. Kane, and E. J. Mele, Phys. Rev. Lett. **98**, 106803 (2007).
[3] M. Z. Hasan and C. L. Kane, Rev. Mod. Phys. **82**, 3045 (2010).
[4] A. Bansil, H. Lin, and T. Das, Rev. Mod. Phys. **88**, 021004 (2016).
[5] S. Ryu, A. P. Schnyder, A. Furusaki, and A. W. Ludwig, New Journal of Physics **12**, 065010 (2010).
[6] C. Kane and T. Lubensky, Nature Physics **10**, 39 (2014).
[7] R. Süsstrunk and S. D. Huber, Science **349**, 47 (2015).
[8] Y. Hadad, J. C. Soric, A. B. Khanikaev, and A. Alù, Nature Electronics **1**, 178 (2018).
[9] F. Li, X. Huang, J. Lu, J. Ma, and Z. Liu, Nature Physics **14**, 30 (2018).
[10] C. W. Duncan, P. Öhberg, and M. Valiente, Phys. Rev. B **95**, 125104 (2017).
[11] D. Zhou and J. Zhang, Phys. Rev. Research **2**, 023173 (2020).
[12] J. Vila, G. H. Paulino, and M. Ruzzene, Phys. Rev. B **99**, 125116 (2019).
[13] E. Prodan and C. Prodan, Phys. Rev. Lett. **103**, 248101 (2009).
[14] J. Ma, D. Zhou, K. Sun, X. Mao, and S. Gonella, Phys. Rev. Lett. **121**, 094301 (2018).
[15] D. Smirnova, D. Leykam, Y. Chong, and Y. Kivshar, Applied Physics Reviews **7**, 021306 (2020).
[16] L. M. Nash, D. Kleckner, A. Read, V. Vitelli, A. M. Turner, and W. T. Irvine, Proceedings of the National Academy of Sciences **112**, 14495 (2015).
[17] D. Zhou, L. Zhang, and X. Mao, Phys. Rev. Lett. **120**, 068003 (2018).
[18] D. Zhou, L. Zhang, and X. Mao, Phys. Rev. X **9**, 021054 (2019).
[19] Y. Hadad, A. B. Khanikaev, and A. Alù, Phys. Rev. B **93**, 155112 (2016).
[20] R. Chaunsali and G. Theocharis, Phys. Rev. B **100**, 014302 (2019).
[21] R. K. Pal, J. Vila, M. Leamy, and M. Ruzzene, Phys. Rev. E **97**, 032209 (2018).
[22] J. Zak, Phys. Rev. Lett. **62**, 2747 (1989).
[23] N. G. Van Kampen, *Stochastic processes in physics and chemistry*, Vol. 1 (Elsevier, 1992).
[24] B. Meerson, Rev. Mod. Phys. **68**, 215 (1996).
[25] B. G.-g. Chen, N. Upadhyaya, and V. Vitelli, Proceedings of the National Academy of Sciences **111**, 13004 (2014).
[26] D. Zhou, J. Ma, K. Sun, S. Gonella, and X. Mao, Phys. Rev. B **101**, 104106 (2020).
[27] J. D. Crawford, Rev. Mod. Phys. **63**, 991 (1991).
[28] W. P. Su, J. R. Schrieffer, and A. J. Heeger, Phys. Rev. Lett. **42**, 1698 (1979).
[29] J. P. Eckmann and D. Ruelle, Rev. Mod. Phys. **57**, 617 (1985).
[30] E. G. Altmann, J. S. E. Portela, and T. Tél, Rev. Mod. Phys. **85**, 869 (2013).
[31] M. Scalora, M. S. Syrchin, N. Akozbek, E. Y. Poliakov, G. D'Aguanno, N. Mattiucci, M. J. Bloemer, and A. M. Zheltikov, Phys. Rev. Lett. **95**, 013902 (2005).
[32] N. Lazarides and G. P. Tsironis, Phys. Rev. E **71**, 036614 (2005).
[33] R. K. Narisetti, M. J. Leamy, and M. Ruzzene, Journal of Vibration and Acoustics **132** (2010).
[34] R. Zaera, J. Vila, J. Fernandez-Saez, and M. Ruzzene, International Journal of Non-Linear Mechanics **106**, 188 (2018).
[35] A. F. Vakakis, L. I. Manevitch, Y. V. Mikhlin, V. N. Pilipchuk, and A. A. Zevin, *Normal modes and localization in nonlinear systems* (Springer, 2001).
[36] M. D. Fronk and M. J. Leamy, Journal of Vibration and Acoustics **139** (2017).
[37] D. Xiao, M.-C. Chang, and Q. Niu, Rev. Mod. Phys. **82**, 1959 (2010).
[38] J. Liu, B. Wu, and Q. Niu, Phys. Rev. Lett. **90**, 170404 (2003).
[39] H. Pu, P. Maenner, W. Zhang, and H. Y. Ling, Phys. Rev. Lett. **98**, 050406 (2007).
[40] J. Liu and L. B. Fu, Phys. Rev. A **81**, 052112 (2010).
[41] L. Renson, G. Kerschen, and B. Cochelin, Journal of Sound and Vibration **364**, 177 (2016).
[42] S. N. Ha, Computers & Mathematics with Applications **42**, 1411 (2001).

- [43] M. Peeters, R. Vigié, G. Sérandour, G. Kerschen, and J.-C. Golinval, in *26th International Modal Analysis Conference, Orlando, 2008* (2008).
- [44] T. Detroux, L. Renson, and G. Kerschen, in *Nonlinear Dynamics, Volume 2* (Springer, 2014) pp. 19–34.
- [45] X. Zhou, Y. Wang, D. Leykam, and Y. D. Chong, *New Journal of Physics* **19**, 095002 (2017).
- [46] D. N. Christodoulides and R. I. Joseph, *Opt. Lett.* **13**, 794 (1988).
- [47] W. A. Benalcazar, B. A. Bernevig, and T. L. Hughes, *Science* **357**, 61 (2017).
- [48] H. Luther, *Mathematics of Computation* **22**, 434 (1968).
- [49] G. D'Aguanno, N. Mattiucci, and M. J. Bloemer, *JOSA B* **25**, 1236 (2008).